

# Angle and Volume Studies in Quantized Space

Michael Seifert  
Swarthmore College

March 19, 2000

## Abstract

The search for a quantum theory of gravity is one of the major challenges facing theoretical physics today. While no complete theory exists, a promising avenue of research is the *loop quantum gravity* approach. In this approach, quantum states are represented by *spin networks*, essentially graphs with weighted edges. Since general relativity predicts the structure of space, any quantum theory of gravity must do so as well; thus, “spatial observables” such as area, volume, and angle are given by the eigenvalues of Hermitian operators on the spin network states. We present results obtained in our investigations of the angle and volume operators, two operators which act on the vertices of spin networks. We find that the minimum observable angle is inversely proportional to the square root of the total spin of the vertex, a fairly slow decrease to zero. We also present numerical results indicating that the angle operator can reproduce the classical angle distribution. The volume operator is significantly harder to investigate analytically; however, we present analytical and numerical results indicating that the volume of a region scales as the  $3/2$  power of its bounding surface, which corresponds to the classical model of space.

# Contents

<b>1</b>	<b>Introduction</b>	<b>1</b>
<b>2</b>	<b>Theory of Loop Quantization</b>	<b>4</b>
2.1	Canonical Electrodynamics . . . . .	4
2.2	The Vector Potential, Holonomies & the Aharonov-Bohm effect . . . . .	7
2.3	Holonomies and Reconstruction Theorems . . . . .	11
2.4	Canonical variables & holonomies in general relativity . . . . .	12
<b>3</b>	<b>Spin Networks</b>	<b>16</b>
3.1	Definition & Properties . . . . .	16
3.2	Intertwiner Bases & Recoupling Theory . . . . .	18
3.3	Spin Networks & Angular Momentum Coupling . . . . .	22
3.4	Spin Networks & Holonomies . . . . .	24
3.5	Operators on Spin Networks . . . . .	27
3.5.1	Angular Momentum Operators . . . . .	27
3.5.2	The Area Operator . . . . .	29
3.5.3	The Angle Operator . . . . .	30
3.5.4	The Volume Operator . . . . .	32
<b>4</b>	<b>The Angle Operator</b>	<b>36</b>
4.1	Spectrum of the Angle Operator . . . . .	36
4.2	Mean Angular Resolution . . . . .	42
4.3	Angle Distribution . . . . .	44
<b>5</b>	<b>The Volume Operator</b>	<b>50</b>
5.1	The $W$ -matrix and Eigenvalue Bounds . . . . .	50
5.2	Volume Eigenvalue Bounds for 4-valent Vertices . . . . .	52
5.3	Eigenvalue Bounds for $n$ -Valent Vertices . . . . .	54
<b>6</b>	<b>Discussion</b>	<b>59</b>
<b>7</b>	<b>Conclusion</b>	<b>62</b>
	<b>Appendices</b>	<b>64</b>
<b>A</b>	<b>Dirac-Bergmann Constraint Analysis</b>	<b>64</b>
A.1	The Generalized Hamiltonian . . . . .	64
A.2	Dirac-Bergmann Analysis & Electrodynamics . . . . .	69
<b>B</b>	<b>Simple Spin Networks and their Values</b>	<b>74</b>
<b>C</b>	<b>Relations Between Wigner <math>6-j</math> Symbols and Kauffman-Lins <math>6-j</math> Symbols</b>	<b>76</b>
<b>D</b>	<b>Diffeomorphism Invariance &amp; the Angle Spectrum</b>	<b>77</b>

<b>Acknowledgements</b>	<b>80</b>
<b>References</b>	<b>80</b>

# 1 Introduction

Most scientists would probably consider the two “great theories” of twentieth-century physics to be Einstein’s theory of general relativity and the theory of quantum mechanics pioneered by Bohr, Heisenberg, and Schrödinger. General relativity describes the interaction of matter and energy with the fabric of spacetime (we experience this interaction as gravity), and accurately predicts the large-scale structure of the Universe. Quantum mechanics, on the other hand, deals with small-scale interactions between matter and energy, successfully explaining the properties of electron, atoms, and other minutia.

General relativity, in some sense, could be considered as the last of the classical theories of physics: it considers space and time to be continuous, and, with sufficient information about the current state of a system, allows us to predict the results of any future experiments with certainty. This is at odds with quantum mechanics, which often requires observable quantities to have discrete spectra; which says (by the Uncertainty Principle) that one’s knowledge of complementary variables will always have a certain degree of uncertainty — we simply *cannot* have complete information about the current state of a system; and which only allows us to predict the probabilities of experimental results.

One would hope, then, that there would be some way of reconciling these two world-views. The program pursued by theoretical physicists since the establishment of quantum mechanics has been, given a classical theory, to attempt to construct a quantum theory which has the known classical theory as its large-scale limit; this process is commonly known as *quantization*. In the case of electrodynamics, the other major classical field theory, this program has been successful: the theory of quantum electrodynamics (also known as QED) was formulated in the 1950s by Feynman, Schwinger, and Tomonaga. Out of QED grew the *Standard Model*, which includes not only electromagnetism but also the strong and weak nuclear forces (which have no corresponding classical theories).

However, there does not yet exist a consistent quantum theory of gravity. This is partly due to a dearth of experimental data around which to build a theory. To obtain data to help us in this quest, we would have to devise an experiment which would (directly or indirectly) measure the gravitational interaction on a small scale. This pursuit is stymied, however, by the incredible weakness of the gravitational force compared to the other three forces of the Standard Model on these scales. An illustration of the vast difference between the strength of the electrostatic force and the gravitational force is attributed to Feynman: If you jumped off the Empire State Building, the gravitational force between you and the Earth would accelerate you to a speed of about 80 m/s over the 350-metre height of the building. However, when you hit the ground, the electrostatic repulsion between the molecules in your body and the molecules in the sidewalk would *decelerate* you an equal amount over less than a centimetre — a minuscule distance.

Moreover, the scales on which quantum gravitational effects might possibly be observed are minuscule. The fundamental constants governing a quantum theory of gravity are  $\hbar$  (Planck’s constant),  $c$  (the speed of light), and  $G$  (the

gravitational constant.) If we express the units of each of these constants in terms of length, mass, and time, we obtain:

$$\begin{aligned}\hbar &\rightarrow \frac{(\text{mass})(\text{length})^2}{\text{time}} \\ c &\rightarrow \frac{\text{length}}{\text{time}} \\ G &\rightarrow \frac{(\text{length})^3}{(\text{mass})(\text{time})^2}\end{aligned}$$

Playing around with these constants, we discover that the only way to create a quantity with dimensions of length is

$$l_0 = \sqrt{\frac{\hbar G}{c^3}} \approx 1.62 \times 10^{-35} \text{ m.} \quad (1.1)$$

This length, known as the *Planck length*, is the scale on which most researchers expect to observe quantum gravitational effects. This is an incredibly minuscule distance; as a basis for comparison, the radius of a proton is on the order of  $10^{-15}$  metres, a full *twenty* orders of magnitude larger! This fact adds to the difficulties in finding any experimental data to guide the search for a quantum theory of gravity.

Undeterred by this lack of physical data, many physicists have proposed theories which attempt to reconcile quantum mechanics with general relativity. Some of these theories (which will not concern us here) attempt to expand or modify the Standard Model to include gravity; these approaches include the popular theories collectively known as *string theory*. Other attempts to reconcile quantum mechanics and general relativity are more conservative, merely attempting to construct a theory of quantum gravity without worrying about the forces included in the Standard Model (at least for the moment.) The theory we will be dealing with in this work falls into the latter category: it attempts only to create a quantum theory with general relativity as its large-scale (“classical”) limit. This is the *loop quantum gravity* approach, in which the fundamental variables of general relativity are encoded in loops (essentially closed paths through space); the observables of this theory then depend only on these loops.

Since general relativity makes predictions about the structure of space, we would expect that this theory would make predictions about the structure of space on a small scale.<sup>1</sup> In particular, this theory makes predictions about the possible values one could observe for such “spatial observables” as areas, angles,

---

<sup>1</sup> The reader may note here that general relativity does not just predict the structure of space, but the structure of spacetime. However, the theory of loop quantum gravity (as we will consider it) is a *canonical* theory, i.e. it requires a separation of the kinematics and the dynamics of the system. As a result, we will only consider the states of the system (corresponding to space only), and not their evolution. We must also point out here that while some theories of the dynamics of spin networks have been put forward, their time-evolution is still not fully understood.

lengths, and volumes. In this work, we will describe recent research into to the spectra of operators corresponding to angle and volume.

Note that this work is intended to be understandable to the reader *without* any significant background in general relativity. As a result, a large portion of the initial theory (Section 2) is couched in terms of a theory the average reader may be more familiar with, namely electrodynamics; in Section 2.4, we make the connection to general relativity by (qualitatively) describing the major differences encountered in applying the described procedures to general relativity. In Section 3, we describe *spin networks*, a complete and sufficient basis for the states of loop quantization theory, as well as the actions of operators on this basis.

Finally, in Sections 4 and 5, we describe the results obtained in our research on the angle and volume operators, respectively. In particular, we find that the minimum observable angle for a given vertex is inversely proportional to the square root of its total spin — a fairly slow convergence to zero. We also calculate the “resolution” of angles around a vertex given its total spin, and show that the distribution of angles around a vertex with sufficient total spin approximates the classical distribution. The complexity of the volume operator hinders any serious analytical work; however, we do use numerical methods to show that the volume of a region seems to scale as the  $3/2$  power of the area of its bounding surface, which is also expected classically.

## 2 Theory of Loop Quantization

### 2.1 Canonical Electrodynamics

As stated in the introduction, we will begin by examining loop quantization theory in the context of classical electrodynamics. The fundamental equations of electrodynamics are, of course, Maxwell's equations:

$$\begin{aligned}\nabla \cdot \mathbf{E} &= 0 & \nabla \times \mathbf{B} - \frac{1}{c} \frac{\partial \mathbf{E}}{\partial t} &= 0 \\ \nabla \cdot \mathbf{B} &= 0 & \nabla \times \mathbf{E} + \frac{1}{c} \frac{\partial \mathbf{B}}{\partial t} &= 0\end{aligned}\tag{2.1}$$

(note that here and throughout this section, we will be working with the source-free equations in Gaussian units.) The symmetry of these equations is striking; if we replace  $\mathbf{E}$  with  $\mathbf{B}$  and  $\mathbf{B}$  with  $-\mathbf{E}$ , the equations are unchanged. One might wonder, then, what the source of this symmetry might be.

To answer this question, we need to return to one of the fundamental properties of  $\mathbf{E}$  and  $\mathbf{B}$ : their definition as vectors. We can define any vector  $\mathbf{x}$  in terms of its (Cartesian) coordinates  $(x^1, x^2, x^3)$ .<sup>2</sup> In this case,

$$\mathbf{x} = x^1 \hat{e}_1 + x^2 \hat{e}_2 + x^3 \hat{e}_3\tag{2.2}$$

To save effort, we will introduce the *Einstein summation convention* here: if an index is repeated in an expression, then we interpret this as summation over all possible values of that index. Using this convention, the previous equation becomes

$$\mathbf{x} = x^i \hat{e}_i\tag{2.3}$$

Special relativity, however, tells us that we must also consider an event's position in time (not just in space.) To take this into account, we modify the conventional idea of a vector to create a *four-vector*; instead of having a component for each of the  $x$ -,  $y$ -, and  $z$ -directions, a four-vector also has a component for the  $t$ -direction. We will denote these components as  $x^0 = ct$ ,  $x^1 = x$ ,  $x^2 = y$ , and  $x^3 = z$ . An event with spacetime coordinates  $(x^0, x^1, x^2, x^3)$  can then be written as

$$\mathbf{x} = x^\mu \hat{e}_\mu\tag{2.4}$$

In general, we will use Greek indices such as  $\mu, \nu, \dots$  to denote components that must be summed over space and time, while Roman indices such as  $i, j, k, \dots$  will denote summation over space only.

Special relativity tells us that if we switch between two frames travelling at a relative velocity  $\beta = v/c$  to each other in the  $x$ -direction, the components of

---

<sup>2</sup> Note that these superscripts are merely indices, not powers of  $x$ .



a spacetime event  $\mathbf{x}$  will transform as

$$\begin{aligned}\bar{x}^0 &= \gamma(x^0 - \beta x^1) \\ \bar{x}^1 &= \gamma(-\beta x^0 + x^1) \\ \bar{x}^2 &= x^2 \\ \bar{x}^3 &= x^3\end{aligned}\tag{2.5}$$

where the “barred” components are in the frame to which we are transforming. Using the summation convention outlined above, we can write (2.5) as a single equation:

$$\bar{x}^\mu = \Lambda_\nu^\mu x^\nu,\tag{2.6}$$

where  $\Lambda$  is the Lorentz transformation matrix

$$\Lambda = \begin{pmatrix} \gamma & -\gamma\beta & 0 & 0 \\ -\gamma\beta & \gamma & 0 & 0 \\ 0 & 0 & 1 & 0 \\ 0 & 0 & 0 & 1 \end{pmatrix},\tag{2.7}$$

and  $\Lambda_\nu^\mu$  is the component of the  $\mu$ th row and the  $\nu$ th column of this matrix.

If  $\mathbf{E}$  and  $\mathbf{B}$  are really vectors, then, they should transform according to equation (2.6). However, a Lorentz transformation on a given electromagnetic field gives the components of the transformed fields as

$$\begin{aligned}\bar{E}_x &= E_x & \bar{E}_y &= \gamma(E_y - \beta B_z) & \bar{E}_z &= \gamma(E_z + \beta B_y) \\ \bar{B}_x &= B_x & \bar{B}_y &= \gamma(B_y + \beta E_z) & \bar{B}_z &= \gamma(B_z - \beta E_y)\end{aligned}\tag{2.8}$$

— not at all a simple Lorentz transformation like those mentioned above.

The way that the components of  $\mathbf{E}$  and  $\mathbf{B}$  mix suggests that these two fields are really part of a larger entity. As it happens, they are components of a second-rank tensor. Such a tensor has sixteen components, which we can denote in an array:<sup>3</sup>

$$F_{\mu\nu} \longrightarrow \begin{pmatrix} F_{00} & F_{01} & F_{02} & F_{03} \\ F_{10} & F_{11} & F_{12} & F_{13} \\ F_{20} & F_{21} & F_{22} & F_{23} \\ F_{30} & F_{31} & F_{32} & F_{33} \end{pmatrix}\tag{2.9}$$

Theoretically, each one of these components could be different; however, such an object has 16 degrees of freedom, whereas we only have six to account for from  $\mathbf{E}$  and  $\mathbf{B}$ . As it happens, if we require  $F_{\mu\nu}$  to be antisymmetric (i.e.  $F_{\mu\nu} = -F_{\nu\mu}$ ),

<sup>3</sup> Note that, technically, this tensor should not be considered a matrix, since it has two lowered indices; if we were to multiply it by a four-vector  $x^\mu$  as in (2.6), we would not obtain another vector  $y^\nu$ .

such a tensor would only have six degrees of freedom:

$$F_{\mu\nu} \longrightarrow \begin{pmatrix} 0 & F_{01} & F_{02} & F_{03} \\ -F_{01} & 0 & F_{12} & F_{13} \\ -F_{02} & -F_{12} & 0 & F_{23} \\ -F_{03} & -F_{13} & -F_{23} & 0 \end{pmatrix} \quad (2.10)$$

How would the components of such a tensor transform under a Lorentz transformation? In analogy to the transformation of vectors in (2.6), we have

$$\bar{F}_{\mu\nu} = \Lambda_{\mu}^{\kappa} \Lambda_{\nu}^{\lambda} F_{\kappa\lambda} \quad (2.11)$$

If we write out the transformations of each component of  $F_{\mu\nu}$  explicitly, we obtain

$$\begin{aligned} \bar{F}_{01} &= F_{01} & \bar{F}_{02} &= \gamma(F_{02} - \beta F_{12}) & \bar{F}_{03} &= \gamma(F_{03} + \beta F_{31}) \\ \bar{F}_{23} &= F_{23} & \bar{F}_{31} &= \gamma(F_{31} - \beta F_{03}) & \bar{F}_{12} &= \gamma(F_{12} + \beta F_{02}) \end{aligned} \quad (2.12)$$

The reader will note that these are exactly the transformations stated in (2.8), suggesting that we can write the electric and magnetic fields together in the *field tensor*  $F_{\mu\nu}$  as

$$F_{\mu\nu} \longrightarrow \begin{pmatrix} 0 & E_x & E_y & E_z \\ -E_x & 0 & B_z & -B_y \\ -E_y & -B_z & 0 & B_x \\ -E_z & B_y & -B_x & 0 \end{pmatrix}. \quad (2.13)$$

We have thus succeeded in combining the electric and magnetic fields into a single tensor  $F_{\mu\nu}$ ; the peculiar transformations of  $\mathbf{E}$  and  $\mathbf{B}$  are merely consequences of the properties of this tensor. However, the symmetry in Maxwell's equations suggests that this is not the only way to put the components of  $\mathbf{E}$  and  $\mathbf{B}$  into a second-rank antisymmetric tensor; we could equally well have constructed the *dual tensor*  $G^{\mu\nu}$ :

$$G^{\mu\nu} \longrightarrow \begin{pmatrix} 0 & B_x & B_y & B_z \\ -B_x & 0 & -E_z & E_y \\ -B_y & E_z & 0 & -E_x \\ -B_z & -E_y & E_x & 0 \end{pmatrix} \quad (2.14)$$

In terms of these new tensors, Maxwell's equations become radically simpler. They are now:

$$\partial_{\nu} F^{\mu\nu} = 0 \quad \text{and} \quad \partial_{\nu} G^{\mu\nu} = 0, \quad (2.15)$$

where we have introduced the operators  $\partial_{\mu} = \partial/\partial x^{\mu}$ . That these equations are equivalent to Maxwell's equations is not entirely evident at first glance, so let us compute a couple of the equations (note that each of the equations above is

really four separate equations, one for each value of  $\mu$ ) to show this equivalence. Consider the first equation when  $\mu = 0$ ; this becomes

$$\begin{aligned}\partial_\nu F^{0\nu} &= \partial_0 F^{00} + \partial_1 F^{01} + \partial_2 F^{02} + \partial_3 F^{03} \\ &= \frac{\partial E_x}{\partial x} + \frac{\partial E_y}{\partial y} + \frac{\partial E_z}{\partial z} \\ &= \nabla \cdot \mathbf{E} = 0,\end{aligned}\tag{2.16}$$

which is Gauss' Law. In the case where  $\mu = 1$ , we have

$$\begin{aligned}\partial_\nu F^{1\nu} &= \partial_0 F^{10} + \partial_1 F^{11} + \partial_2 F^{12} + \partial_3 F^{13} \\ &= -\frac{1}{c} \frac{\partial E_x}{\partial t} + \frac{\partial B_z}{\partial y} - \frac{\partial B_y}{\partial z} \\ &= \left( -\frac{1}{c} \frac{\partial \mathbf{E}}{\partial t} + \nabla \times \mathbf{B} \right)_x = 0\end{aligned}\tag{2.17}$$

which is the  $x$ -component of Ampere's law. The  $\mu = 2$  and  $\mu = 3$  cases of this equation give the  $y$  and  $z$  components of Ampere's law, and the tensor equation for  $G^{\mu\nu}$  gives the two remaining Maxwell's equations.<sup>4</sup>

## 2.2 The Vector Potential, Holonomies & the Aharonov-Bohm effect

To quantize a given theory, we need to decide on a particular set of configuration variables which describe the system. In the simplest example, the quantum theory of a free particle uses the particle's position  $x$  and momentum  $p$  to describe the motion of the particle. In general, we want to find some set of generalized "positions" and "momenta" that can describe all the states of the system; however, doing so is not always easy, since a "natural" set of configuration variables may be related by some set of complicated constraints. A general method for finding the constraints on an arbitrary set of configuration variables was pioneered by Bergmann and Dirac, and is presented in Appendix A, along with its application to electrodynamics. Here, however, we only need to note the final results: the canonical configuration variable for electrodynamics is the vector potential  $\mathbf{A}$ , given by  $\mathbf{B} = \nabla \times \mathbf{A}$ . We will also make use of the four-vector potential, given by

$$A_\mu = (V, A_x, A_y, A_z)\tag{2.18}$$

where  $V$  is the electric potential. The field tensor  $F_{\mu\nu}$  can be written quite elegantly in terms of this four-vector potential:

$$F_{\mu\nu} = \partial_\mu A_\nu - \partial_\nu A_\mu.\tag{2.19}$$

---

<sup>4</sup> This method can be elegantly extended to include field sources (i.e. charges and currents), but this case will not concern us here. The interested reader is referred to Griffiths [1] (from which most of this derivation is taken) for further information.

To successfully quantize this theory, we must also have a conjugate momentum for the chosen configuration variable. Using Bergmann-Dirac canonical analysis, we can show that the “momentum” of the vector potential  $A_a$  is the electric field  $E^a$ .<sup>5</sup> Our two configuration variables are the vector potential and the electric field.

One might ask the question, however, whether the vector potential is necessarily the best choice for a configuration variable, especially since (in the classical theory) only  $\mathbf{B} = \nabla \times \mathbf{A}$  is measurable. Furthermore,  $A_a$  has the distinct disadvantage of possessing gauge freedom: given a vector potential  $A_a$ , we can perform a transformation of the form

$$A_a \rightarrow A_a + \frac{\partial \lambda}{\partial x^a}$$

without affecting the physical state. This freedom is worse than it appears: suppose we have a physical system which we consider under two gauges  $\lambda_1$  and  $\lambda_2$ , the first of which is a function of time and the second of which is not. If we let the system evolve, the two gauges will generally predict different values of  $A_a$  after a given amount of time; hence, our theory does not uniquely predict the time-evolution of the configuration of the system. If we insist on treating  $A_a$  as a fundamental variable, then, we must abandon determinism — a step that we are loath to take. Further, this interpretation does not prohibit causal influences from travelling faster than light; in theory, a change in the field can cause an instantaneous change arbitrarily far away. Thus, interpreting  $A_a$  as a fundamental field forces us to eliminate determinism and causality, two of the most basic tenets of physics.

In the face of this, most people would interpret  $\mathbf{B} = \nabla \times \mathbf{A}$  (and  $\mathbf{E}$ ) as physical fields; this is the standard classical interpretation. This interpretation has the advantage of being deterministic (since gauge transformations do not change  $\mathbf{B}$ ) and limiting causal influences to the speed of light. Indeed, if we are defining our fields on a “well-behaved” chunk of space, or only examining classical phenomena, then the choice of  $\mathbf{B}$  as the fundamental variable is natural, and explains everything that needs explaining.<sup>6</sup>

As the reader might have guessed from the above caveat, however, there are quantum effects that seem to contradict the primacy of  $\mathbf{B}$ . The best-known of these is the *Aharonov-Bohm effect*. In this experiment, a beam of charged particles with charge  $e$  is sent through a double-slit interference experiment (see Figure 1.) Between the slits we place an impenetrable solenoid (i.e. the particles’ wave functions are zero inside the solenoid.)

Theory predicts that a particle travelling along a given path  $\gamma$  will change

---

<sup>5</sup> Note that in this equation, the components of  $E$  have a superscript instead of a subscript; this is due to the difference between covariant and contravariant tensors. In this case, however, raising or lowering an index simply introduces a minus sign if and only if the index is 0 (i.e.  $x^0 = -x_0$ , but  $x^1 = x_1$ .)

<sup>6</sup> The reader might wonder what we might possibly mean by “well-behaved”; this will become evident shortly.

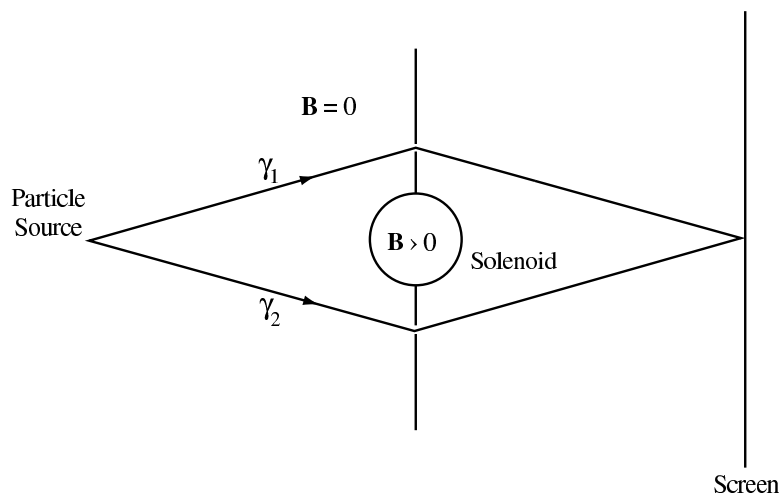


Figure 1: The Aharonov-Bohm experiment. Particles are sent through a double-slit apparatus and create an interference pattern on the screen. The presence of the solenoid creates a phase difference between the two paths  $\gamma_1$  and  $\gamma_2$ , which affects the interference pattern. Note that although the magnetic field is *zero* in the region where the particle travels, the solenoid still has an effect on the particles.

its phase factor:

$$|\phi(t)\rangle = \exp \left[ \frac{-iEt}{\hbar} + \frac{ie}{\hbar c} \oint_{\gamma} A_i dx^i \right] \quad (2.20)$$

where  $E$  is the energy of the particles. The first part of the phase factor corresponds to the normal time-evolution of the state; the second part arises solely from the vector potential due to the solenoid (even though the particle is moving in a region of no magnetic field.) This phase factor will have observable consequences in the interference pattern on the screen behind the slits. For example, the phase difference between the two paths at the centre of the screen (i.e. equal time for both paths) will be given by

$$\begin{aligned} \Delta\phi &= \frac{e}{\hbar c} \int_{\gamma_1} A_i dx^i - \frac{e}{\hbar c} \int_{\gamma_2} A_i dx^i \\ &= \frac{e}{\hbar c} \oint_{\gamma} A_i dx^i \end{aligned} \quad (2.21)$$

where  $\gamma$  is the closed loop created by travelling along  $\gamma_1$ , then along  $\gamma_2$  in reverse. The integrand of this equation can be expressed more familiarly as  $\mathbf{A} \cdot d\mathbf{x}$ ; we can thus apply Stokes' Law to this to give

$$\begin{aligned} \Delta\phi &= \frac{e}{\hbar c} \int_S \nabla \times \mathbf{A} \cdot d\mathbf{S} \\ &= \frac{e\Phi}{\hbar c} \end{aligned} \quad (2.22)$$

where  $\gamma$  is the border of the new surface  $S$ , and  $\Phi = \int \mathbf{B} \cdot d\mathbf{S}$  is the magnetic flux through this surface (which is equal to the flux through the solenoid, since  $\mathbf{B} = 0$  outside it.)

This experiment has been performed (the experimenters measured shifts in the interference pattern as  $\Phi$  was increased); the results confirm the theoretical prediction, that the interference pattern does indeed depend on  $\int \mathbf{A} \cdot d\mathbf{x}$ . This result seems to catch us in a contradiction. On the one hand, choosing the vector potential  $A^\mu$  as a fundamental configuration variable forces us to abandon determinism and causality; on the other hand, the Aharonov-Bohm effect suggests that the vector potential holds some physical importance. Without a third option, we are forced to choose the former — while a non-deterministic theory is not very nice, one that doesn't correspond to the physical world is worthless.

Fortunately, a third option does exist: *holonomies*. Recall that the observable result of the Aharonov-Bohm effect is not dependent on the vector potential *per se*, but instead on its path integral as defined in (2.21). Thus, given a path in space  $\gamma$ , we define the holonomy of  $\gamma$  to be

$$\begin{aligned} U_{\gamma} &= \exp \left[ ig \int_0^1 A_i(\gamma(t)) \dot{\gamma}^i(t) dt \right] \\ &= \exp \left[ ig \int_{\gamma} A_i dx^i \right] \end{aligned} \quad (2.23)$$

where  $g$  is a coupling constant to make the argument of the exponential dimensionless. The reader will note that if we set  $g = e/\hbar c$ , this factor reduces to that given in the second term of (2.20).

We can thus escape our earlier dilemma by regarding the holonomies as the fundamental configuration variables. The consequences of doing this are discussed at length in an excellent article by Belot [2]. He notes that the holonomies, like  $\mathbf{B}$ , are gauge-invariant; however, they possess another important, related quality which the magnetic field does not. In a chunk of “well-behaved” space, two fields correspond to the same  $\mathbf{B}$  field if and only if they differ by one of the usual gauge transformations (i.e. a term of the form  $\partial\lambda/\partial x^a$  for some  $\lambda$ .) This is because normal Euclidean space is *simply connected*: any loop in space (i.e. a path through space that begins and ends at the same point) can be contracted continuously to a point. However, if a space is not simply connected, then there are non-gauge transformations that are interpreted as identical  $\mathbf{B}$  fields. The holonomies, on the other hand, do not have this problem; this is thus a point in their favour.<sup>7</sup>

However, using the holonomies as the fundamental variables of the theory violates locality in an even more fundamental way than our first interpretation. Instead of considering the field  $A_a$  at a collection of points, we must now consider the values of the field over a region with actual spatial extent; this means that if we don’t know the field *everywhere*, we cannot determine all of the possible holonomies. The philosophical issues this fact raises are fascinating, but are unfortunately not the primary concern of this paper; the interested reader is encouraged to consult Belot’s paper for more information on this subject.

### 2.3 Holonomies and Reconstruction Theorems

We have shown that the construction of a quantum theory from the canonical variables  $A_a$  and  $E^a$  depends in some way on holonomies; we will now make this notion somewhat more formal. We define a path  $\gamma$  on a space  $\Sigma$  to be a continuous map from the closed unit interval  $[0, 1]$  to  $\Sigma$ . In the case of Euclidean space we can think of  $\Sigma$  as equivalent to  $\mathbf{R}^3$ ; however,  $\Sigma$  may equally well be a “curved” manifold, as in general relativity. If the property  $\gamma(0) = \gamma(1)$  holds, then we say that  $\gamma$  is a *closed loop*.

Given a (not necessarily closed) path  $\gamma$  and a vector potential  $A_a$ , we can then define a holonomy  $U_\gamma$  of the path  $\gamma$ :

$$\begin{aligned} U_\gamma &= \exp \left[ ig \int_0^1 A_a(\gamma(t)) \dot{\gamma}^a(t) dt \right] \\ &= \exp \left[ ig \int_\gamma A_a dx^a \right] \end{aligned} \tag{2.24}$$

where  $g$  is merely a coupling constant introduced to make the argument of the

---

<sup>7</sup>The reader who might be wondering if non-simply-connected spaces actually correspond to any physical situations is reminded that the Aharonov-Bohm effect takes place in such a space — a loop around the solenoid cannot be contracted “through” the solenoid.

exponential dimensionless. In other words, the holonomy of a given path is merely (in this simple case) the exponential of  $i$  times the path integral of the vector potential along the path in question.

An important feature of closed-loop holonomies is that it is generally possible to reconstruct the vector potential from them; in other words, the representation of the vector potential in terms of its holonomies and in terms of the field itself are completely equivalent. The conditions under which this holds are the subject of mathematical *reconstruction theorems*. We will not go into detail on how the existence of a vector potential corresponding to a given set of loops is proven, nor the actual process of the reconstruction itself; for more details, the interested reader is referred to Barrett [3] or Giles [4].

## 2.4 Canonical variables & holonomies in general relativity

Before we examine the nature of the spin networks mentioned in Section 2.3, we must discuss the difficulties in applying this technique to Einstein’s theory of general relativity. As originally conceived by Einstein, general relativity consisted of a spacetime manifold  $\Sigma$ , at each point of which a metric  $g_{\mu\nu}$  is defined. Early attempts to quantize general relativity used the metric as one of the parameters of the configuration space. Unfortunately, this approach failed, mainly because the constraints generated by this approach (as in Appendix A) were intractable.

There the matter rested until the 1986, when Ashtekar [5, 6] and Sen [7] reformulated general relativity in terms of the so-called “new variables”. In this formulation, the metric was no longer the fundamental variable of the theory. Instead, the two variables used in this new formulation are the *connection*  $A_a^i(x)$  (akin to the vector potential in electrodynamics) and the *inverse densitized triad*  $E_i^a(x)$  (akin to the electric field). As our notation would suggest, the connection is viewed as the configuration variable (akin to the vector potential), while the inverse densitized triad is its canonically conjugate momentum. These quantities have “clean” Poisson brackets, as we require:

$$\{E_i^a(x), E_j^b(y)\} = 0 \quad (2.25)$$

$$\{A_a^i(x), A_b^j(y)\} = 0 \quad (2.26)$$

$$\{A_a^i(x), E_j^b(y)\} = \beta G \delta_i^j \delta_a^b \delta^3(x - y) \quad (2.27)$$

For those readers familiar with general relativity, we can also express these variables in terms of more familiar quantities.  $E_i^a$  is related to the metric of constant-time surfaces  $q_{ab}$  by

$$|q|q^{ab} = E_i^a E_i^b, \quad (2.28)$$

where  $q_{ab}$  is the spatial part of the metric and  $|q|$  is the determinant of  $q_{ab}$ . We can also express these in terms of the triad from the ADM formalism:

$$E_i^a = \sqrt{|q|} e_i^a \quad (2.29)$$



The connection  $A_a^i(x)$  can be expressed as

$$A_a^i = \Gamma_a^i + \beta K_a^i, \quad (2.30)$$

where  $\Gamma_a^i$  is the connection associated with the (undensitized) triad (defined by  $\partial_{[a} e_{b]}^i = \Gamma_{[a}^i e_{b]}^j$ ),  $K_a^i$  is the extrinsic curvature of the 3-surface, and  $\beta$  is an as-yet undetermined parameter known as the *Immiri parameter*, first put forward in [8].

While there is a resemblance between electrodynamics and general relativity in this regard, there are also differences (of course) between these two theories. The reader will no doubt have noticed by now that our relativistic variables bear an extra index (i.e.  $i, j, \dots$ ). This index corresponds to the *internal space* of the configuration variables. Each point on  $\Sigma$  has an internal space associated with it; a vector based at a given point can be thought of as existing in this space. Since two vectors at two different points exist in different spaces, they cannot immediately be compared. We need to define some self-consistent way of comparing two objects at two different points; this, as it turns out, is done by the connection  $A_a^i$ .

Suppose, then, we take a vector at some point  $x_0$  on the manifold, and attempt to move it around the loop (using the connection  $A_a^i$  to translate from the neighbourhood of each point to the manifold.) This movement will be performed in such a way that as the vector passes through a small neighbourhood of each point, it will point in the same direction. This process is called *parallel transport*, since the vector stays parallel to itself along each infinitesimal segment.

Transporting a vector around a loop in this way does not always yield a vector that is parallel to the original vector — even if we keep the vector parallel to itself along each “step of the way.” In the special case of flat space, the parallel-transported vector is equivalent to the original vector. However, if space has some amount of curvature, we will not necessarily get the same vector back after we transport it around a loop. (For an example of this, see Figure 2, in which a vector is parallel-transported around two different loops on a sphere.) With this in mind, we associate a three-dimensional rotation with each path in  $\Sigma$ ; these rotations will be the holonomies of general relativity. In three dimensions, we can represent these rotations by members of the group  $SO(3)$ , the group of all orthogonal  $3 \times 3$  matrices with determinant 1. However, this group has the same structure as (i.e. is isomorphic to)  $SU(2)$ , the group of all  $2 \times 2$  unitary matrices with determinant 1; since these matrices are simpler, general relativity is more commonly thought of in terms of  $SU(2)$  than in terms of  $SO(3)$ .

This representation of the holonomies in terms of matrices has two important consequences that complicate the simple derivation we used for canonical electrodynamics. The first complication arises from the structures of the groups used in each theory. In the case of canonical electrodynamics, the holonomies were complex numbers of unit modulus; these can be thought of, in the interest of drawing parallels, as members of  $U(1)$  (the set of all unitary  $1 \times 1$  matrices.)

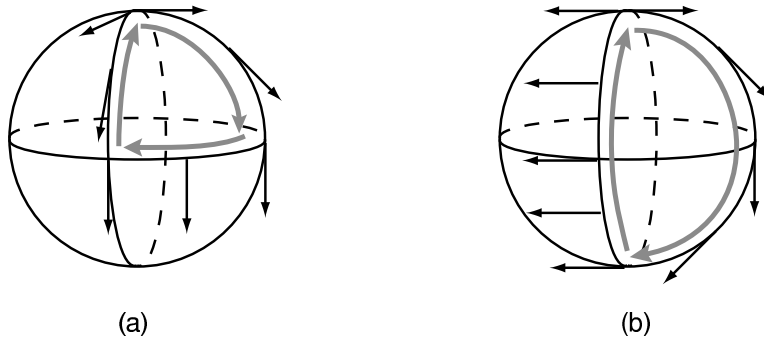


Figure 2: Parallel transport of vectors on a non-flat surface. In (a), the vector is transported from the north pole to the equator, 90 degrees along the equator, and back to the north pole; the resulting vector is rotated by 90 degrees. In (b), the vector is transported from the north pole to the south pole along a line of longitude, and back to the north pole along another line of longitude 90 degrees from the first; the resulting vector is rotated by 180 degrees. Note that the vector has been transported “parallel to itself” at each point; it is the curvature of the surface itself that causes these rotations.

$U(1)$  happens to be a simple group, in that any two elements  $a, b \in U(1)$  commute (i.e.  $ab = ba$ .) However,  $SU(2)$  is not so simple; in general, elements of  $SU(2)$  do not commute (i.e.  $ab \neq ba$ .)<sup>8</sup> Because of this, it turns out that we can no longer use the simple equation in (2.23) to find the holonomy. Instead of simply taking the exponential of a path integral, we must use the *path-ordered exponential* defined as

$$\begin{aligned}
 U_\gamma[A] &= \mathcal{P} \exp \left[ \int_0^1 A_a(\gamma(t)) \dot{\gamma}^a(t) dt \right] \\
 &= 1 + \sum_{n=1}^{\infty} \int_0^1 dt_1 \int_{t_1}^1 dt_2 \cdots \int_{t_{n-1}}^1 dt_n \\
 &\quad \times A_{a_n}(\gamma(t_n)) \cdots A_{a_1}(\gamma(t_1)) \dot{\gamma}^{a_n}(t_n) \cdots \dot{\gamma}^{a_1}(t_1)
 \end{aligned}
 \tag{2.31}$$

Readers familiar with time-dependent perturbation theory may recognize this expression as being similar to the time-ordered exponential (also known as the Dyson series.)

The second important complication introduced by the matrix representation arises when we attempt to account for gauge transformations. Under gauge transformations, the holonomies transform as

$$U_\gamma \mapsto U'_\gamma = g^{-1}(\gamma(1)) \cdot U_\gamma \cdot g(\gamma(0))
 \tag{2.33}$$

<sup>8</sup> The reader with a modicum of background in group theory will recognize that  $U(1)$  is *Abelian*, while  $SU(2)$  is *non-Abelian*.

where  $g$  is a smooth  $SU(2)$ -valued function on  $\Sigma$ . This kind of thing just won't do; we want a gauge-invariant quantity. To turn this quantity into such a quantity, we restrict ourselves to closed loops, and take the trace of the holonomy, also known as the *Wilson loop*:

$$T_\gamma = \text{Tr}(U_\gamma) \tag{2.34}$$

This quantity is invariant under gauge transformations:

$$\begin{aligned} T'_\gamma &= \text{Tr}(g^{-1}(\gamma(1)) \cdot U_\gamma \cdot g(\gamma(0))) \\ &= \text{Tr}(g(\gamma(0)) \cdot g^{-1}(\gamma(1)) \cdot U_\gamma) \\ &= \text{Tr}(U_\gamma) = T_\gamma, \end{aligned} \tag{2.35}$$

where we have used the cyclic properties of the trace and the fact that  $\gamma(0) = \gamma(1)$ .

### 3 Spin Networks

The construction of a quantum theory from closed-loop holonomies is known as the *loop quantization* technique. However, there is a problem with loop quantization: the loop basis is overcomplete. In other words, certain linear combinations of closed-loop holonomies are always equal to each other. This means that if we construct a theory out of these loops, we will end up with linearly dependent basis states (since we will not have taken these equalities into account.)

In attempting to resolve this difficulty, Rovelli and Smolin [9] discovered that it could be circumvented entirely by the use of *spin networks*. To construct such a network, we must first make another definition: we define a *graph*  $\Gamma$  as a finite collection  $\{\gamma_1, \gamma_2, \dots, \gamma_n\}$  of smooth curves in  $\Sigma$  that intersect only at their ends (if at all.) With each curve, we associate its holonomy, i.e.

$$U_{\gamma_i}(A) = \mathcal{P} \exp \left[ \int_{\gamma_i} A_a dx^a \right] \quad (3.1)$$

Our quantum states will then be functions of these holonomies:

$$\Psi(A) = f(U_1, U_2, \dots, U_n) \quad (3.2)$$

Since these networks play a central role in our theory, we will take some time to examine them now. Much of the following exposition is taken from Major [10].

#### 3.1 Definition & Properties

Spin networks were first invented by Penrose, [11] and essentially consist of graphs with weighted edges. Their fundamental units are strands, which are defined to be equivalent to  $2 \times 2$  matrices:

$$\delta_A^B = \begin{array}{c} B \\ \curvearrowright \\ A \end{array} \quad \tilde{\epsilon} = i\epsilon^{AB} = \begin{array}{c} A \quad B \\ \cup \end{array} \quad \tilde{\epsilon} = i\epsilon_{AB} = \begin{array}{c} \cup \\ A \quad B \end{array} \quad (3.3)$$

Indeed, any  $2 \times 2$  matrix can be “placed” into a spin network, in the form of a “tagged” line:

$$\psi_A^B = \begin{array}{c} B \\ | \\ \boxed{\Psi} \\ | \\ A \end{array} \quad (3.4)$$

To join two strands together, we multiply two matrices with a common index:

$$\delta_A^B \cdot \tilde{\epsilon}^{BC} \cdot \tilde{\epsilon}_{CD} \cdot \delta_D^E = \begin{array}{c} B \quad C \quad D \\ \cup \quad \cup \\ A \end{array} = \begin{array}{c} E \\ \cup \\ A \end{array} = \delta_A^E \quad (3.5)$$

Using these rules, we can show that these strands behave as would thin strings in a plane, with one exception: the equation  $\delta_A^D \delta_B^C \tilde{\epsilon}_{CD} = -\tilde{\epsilon}_{AB}$  leads us to the odd strand equation

$$\begin{array}{c} \text{C} \\ \diagup \quad \diagdown \\ \text{A} \quad \text{B} \end{array} = \delta_A^D \tilde{\epsilon}_{CD} \delta_B^C = \tilde{\epsilon}_{BA} = -\tilde{\epsilon}_{AB} = - \begin{array}{c} \text{A} \quad \text{B} \\ \diagdown \quad \diagup \end{array} \quad (3.6)$$

To resolve this, we associate a negative sign with each strand crossing. With this modification, the strands of a spin network behave exactly as would thin (i.e. untwistable) threads in a plane.

The mathematical definition of the strands in terms of matrices gives rise to an interesting identity, known as the “binor identity” or the “skein relation.” We recall the matrix identity

$$\epsilon_{AC} \epsilon^{BD} = \delta_A^B \delta_C^D - \delta_A^D \delta_C^B \quad (3.7)$$

When translated into strands, this identity becomes

$$\begin{array}{c} \text{B} \quad \text{D} \\ \diagdown \quad \diagup \\ \text{A} \quad \text{C} \end{array} + \begin{array}{c} \text{B} \quad \text{D} \\ \diagup \quad \diagdown \\ \text{A} \quad \text{C} \end{array} + \begin{array}{c} \text{B} \quad \text{D} \\ | \quad | \\ \text{A} \quad \text{C} \end{array} = 0 \quad (3.8)$$

The fact that a given set of strands may satisfy one or more linear relations (as in the binor identity above) leads us to construct a basis in which such linear relations do not exist. This is accomplished by the use of antisymmetric combinations of multiple strands. The simplest example of such a combination is the 2-strand:

$$\left| \begin{array}{c} | \\ 2 \\ | \end{array} \right\rangle = \frac{1}{2} \left[ \left| \begin{array}{c} | \\ \diagdown \quad \diagup \\ | \end{array} \right\rangle - \left| \begin{array}{c} | \\ \diagup \quad \diagdown \\ | \end{array} \right\rangle \right] \quad (3.9)$$

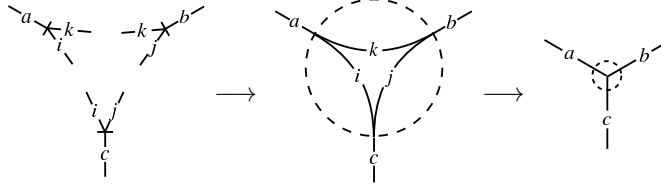
In general, we construct an  $n$ -strand by summing over all permutations of the lines, changing the sign for each strand crossing:

$$\left| \begin{array}{c} | \\ n \\ | \end{array} \right\rangle = \frac{1}{n!} \sum_{\sigma \in S_n} (-1)^{|\sigma|} \left| \begin{array}{c} \dots n \dots \\ \sigma \\ | \end{array} \right\rangle \quad (3.10)$$

where  $\sigma$  stands for a permutation of the lines.<sup>9</sup>

<sup>9</sup> The exact correspondence between elements of  $S_n$  and “permutations of the lines” can be established as follows: represent an element of  $S_n$  by its permutation on  $n$  letters. Write the letters  $12 \dots n$  in a row, and write the permuted letters  $\sigma(1)\sigma(2) \dots \sigma(n)$  just below them. The lines connecting the same elements in the top and bottom rows correspond to the weaving of the strands.

These networks would be boring if they only consisted of simple  $n$ -strands. However, we can define a trivalent vertex of these edges by splitting three  $n$ -strands and reassembling them as follows:



where the labels  $i$ ,  $j$ , and  $k$  are “internal” labels, and are related to the “external” labels  $a$ ,  $b$ , and  $c$  by the relations

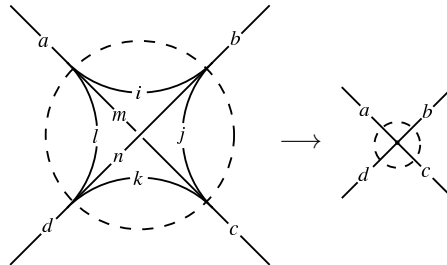
$$\begin{aligned} i &= \frac{1}{2}(a + c - b) \\ j &= \frac{1}{2}(b + c - a) \\ k &= \frac{1}{2}(a + b - c) \end{aligned}$$

The dotted lines in the above diagrams indicate the boundaries between the internal structure of the vertices and the external structure (i.e. the strands themselves.) For these internal edges (and hence the vertex itself) to exist,  $a$ ,  $b$ , and  $c$  must satisfy two conditions. First, the sum  $a + b + c$  must be even; second,  $a$ ,  $b$ , and  $c$  must satisfy the triangle inequalities:

$$a + b \geq c \quad b + c \geq a \quad c + a \geq b$$

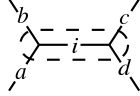
### 3.2 Intertwiner Bases & Recoupling Theory

Even with the existence of trivalent vertices, life is rather boring; we ask ourselves, then, whether it is possible to construct vertices with arbitrary valence. We could try using the same technique we used in constructing the trivalent vertices, by “splitting” the incoming strands and reassembling them in all combinations:



However, we quickly notice that the internal edges are underdetermined: there are six internal edges  $i, j, k, l, m$ , and  $n$ , and only four external edges to determine them. Indeed, for a general  $n$ -valent vertex, there will be  $n(n - 1)/2$  internal edges to be determined by only  $n$  parameters.

While we could still proceed with our analysis using all of the extra internal edges, it will be to our advantage to introduce a different way of denoting the internal edges of a vertex. Since internal edges of a trivalent vertex are completely determined, we will attempt to build a four-valent vertex out of trivalent vertices instead:



Instead of having to deal with a mishmash of internal edges, we will now only have to deal with the one internal edge  $i$ . Indeed, from here on the phrase “internal edges” will be used exclusively to refer to edges such as  $i$ , and not to the “split strands” used to construct the trivalent vertices.

However, this construction is useless if we cannot actually find an edge  $i$  that allows the internal trivalent vertices to be constructed. The first requirement to deal with is the “evenness” requirement. For the trivalent vertices to exist, the restrictions on the triples  $(a, b, i)$  and  $(c, d, i)$  are:

$$a + b \equiv i \pmod{2} \quad \text{and} \quad c + d \equiv i \pmod{2}, \quad (3.11)$$

which together imply that the sum  $a + b + c + d$  must be even. Similarly, from the triangle inequalities  $a + b \geq i$  and  $i + c \geq d$  together imply that  $a + b + c \geq d$ ; we can similarly construct three other inequalities, creating a total of four “generalized” triangle inequalities:

$$\begin{aligned} a + b + c &\geq d \\ a + b + d &\geq c \\ a + c + d &\geq b \\ b + c + d &\geq a \end{aligned} \quad (3.12)$$

Alternately, these four inequalities can be summarized in one statement:

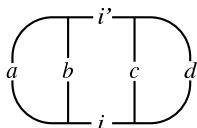
$$a + b + c + d \geq 2x \text{ for } x \in \{a, b, c, d\} \quad (3.13)$$

There is still an ambiguity in the internal edge, however; a bit of thought reveals that the value of  $i$  can lie in the range

$$\max\{|a - b|, |c - d|\} \leq i \leq \min\{a + b, c + d\} \quad (3.14)$$

For example, in the case where  $a = b = c = d$ ,  $i$  can take on any (even) value between 0 and  $2a$ . We can think of these sets of vertices as state vectors, which span the space of all possible four-valent vertices with “external” edges  $a$ ,  $b$ ,  $c$ , and  $d$ .

We can define the inner product between two vertex states by joining together corresponding external edges. For example, if we take the inner product between a state labelled by  $i$  and a state labelled by  $i'$ , we find that it is given by the value of the following network:

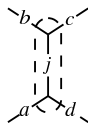


If we apply the “bubble” identity (B.5) to right-hand bubble in this diagram, we find that the value of this diagram is 0 unless  $i = i'$ :

$$\begin{aligned}
 \begin{array}{c} \text{---} i' \text{---} \\ | \quad | \\ a \quad b \quad c \quad d \\ | \quad | \\ \text{---} i \text{---} \end{array} &= \delta_{ii'} \frac{\theta(i, c, d)}{\Delta_i} \begin{array}{c} \text{---} \\ | \quad | \\ a \quad b \\ | \quad | \\ \text{---} i \end{array} \\
 &= \delta_{ii'} \frac{\theta(i, a, b)\theta(i, c, d)}{\Delta_i} \tag{3.15}
 \end{aligned}$$

Thus, these basis states are orthogonal.<sup>10</sup>

The reader may have wondered, back when we were defining the four-valent vertex in terms of internal trivalent vertices, why we chose to do so in this manner. After all, we could have equally well joined together the vertices  $a$  and  $d$  in one internal vertex and the vertices  $b$  and  $c$  in the other:



If we had defined the internal edge in this way, we would have obtained a different set of state vectors; however, it is not immediately evident that these vectors will span the same space as our original set. That these new vectors actually *do* span the same space is a result of the *recoupling theorem* (see Appendix B):

$$\begin{array}{c} \text{---} b \text{---} \\ \diagdown \quad \diagup \\ \text{---} i' \text{---} \\ \diagup \quad \diagdown \\ \text{---} a \text{---} \end{array} \begin{array}{c} \text{---} c \text{---} \\ \diagdown \quad \diagup \\ \text{---} i \text{---} \\ \diagup \quad \diagdown \\ \text{---} d \text{---} \end{array} = \sum_i \left\{ \begin{array}{ccc} a & b & i \\ c & d & i' \end{array} \right\} \begin{array}{c} \text{---} b \text{---} \\ \diagdown \quad \diagup \\ \text{---} i \text{---} \\ \diagup \quad \diagdown \\ \text{---} a \text{---} \end{array} \begin{array}{c} \text{---} c \text{---} \\ \diagdown \quad \diagup \\ \text{---} i \text{---} \\ \diagup \quad \diagdown \\ \text{---} d \text{---} \end{array} \tag{3.16}$$

Thus, given a vertex with an internal decomposition in either form, we can express it as a linear combination of vertices with an internal decomposition of the other form. These internal decompositions are called *intertwiners*; what we have just shown is that the set of all intertwiners of either form is a basis for the space of all intertwiners, and that the recoupling theorem is a transformation between these bases. Moreover, this transformation happens to have a nice property. In [12], De Pietri and Rovelli show that the recoupling theorem is a unitary transformation, i.e. vector norms are preserved under it. We can thus switch back and forth between bases fairly simply; this ability will become

<sup>10</sup>They are certainly not normalized; however, this fact will have no effect on the properties we examine.



$$\begin{aligned}
& \cdots -i_1 \text{---} \overbrace{\text{---} i_2 \text{---}} \text{---} i_3 \text{---} i_4 \text{---} \cdots \\
& \quad \quad \quad \begin{array}{c} | \\ a_1 \\ | \\ \text{---} \\ | \\ a_2 \\ | \\ \text{---} \\ | \\ a_3 \end{array} \\
& = \sum_{j_2} \begin{Bmatrix} a_1 & i_1 & j_2 \\ i_3 & a_2 & i_2 \end{Bmatrix} \\
& \quad \quad \quad \begin{array}{c} \text{---} i_1 \text{---} \overbrace{\text{---} i_3 \text{---}} \text{---} i_4 \text{---} \cdots \\ | \\ j_2 \\ \begin{array}{c} \diagdown \\ a_1 \\ \diagup \\ a_2 \end{array} \\ | \\ a_3 \end{array} \\
& = \sum_{j_2} \sum_{j_3} \begin{Bmatrix} j_2 & i_1 & j_3 \\ i_4 & a_3 & i_3 \end{Bmatrix} \begin{Bmatrix} a_1 & i_1 & j_2 \\ i_3 & a_2 & i_2 \end{Bmatrix} \\
& \quad \quad \quad \begin{array}{c} \text{---} i_1 \text{---} i_4 \text{---} \cdots \\ | \\ j_3 \\ | \\ a_3 \\ | \\ j_2 \\ \begin{array}{c} \diagdown \\ a_1 \\ \diagup \\ a_2 \end{array} \end{array}
\end{aligned}$$

Figure 3: The “branch transformation”, in which an internal branch is added to the intertwiner. Internal edges are marked with  $i$ s and  $j$ s, while external edges are marked with  $a$ s. The gray outlines indicate the internal edge to which the recoupling theorem is applied in the next step.

invaluable to us when we examine the actions of the angle and volume operators in Sections 3.5.3 and 3.5.4, respectively.

We have now defined what we mean by an 4-valent vertex; however, our goal was to create a vertex of arbitrary valence. It is fairly obvious how this can be done: for each new edge we wish to add, we add a trivalent vertex to the intertwiner. Thus, a 5-valent vertex contains three trivalent vertices in its intertwiner, a 6-valent vertex contains four trivalent vertices, and (in general) an  $n$ -valent vertex contains  $n - 2$  trivalent vertices in its intertwiner. It can also be shown that given a set of incoming edges with labels  $\{a_1, a_2, \dots, a_n\}$ , it is possible to create an  $n$ -valent vertex out of them if and only if the following conditions are satisfied:

$$\sum_{i=1}^n a_i \text{ is even} \tag{3.17}$$

$$\sum_{i=1}^n a_i \geq 2a_j \text{ for } 1 \leq j \leq n \tag{3.18}$$

The first of these is the usual “evenness” requirement, while the second is a generalized triangle inequality similar to (3.13).

As might be expected, these higher-valence vertices also have intertwiner bases (although these bases are of much higher dimension.) However, we can again use the recoupling theorem to shift between these bases. There are two general types of these transformations which will be very useful to us later on. The first of these is illustrated in Figure 3, and allows us to transform between bases of different “shapes.” By creating (or, in reverse, removing) branches from an arbitrary internal decomposition, we can transform an intertwiner of

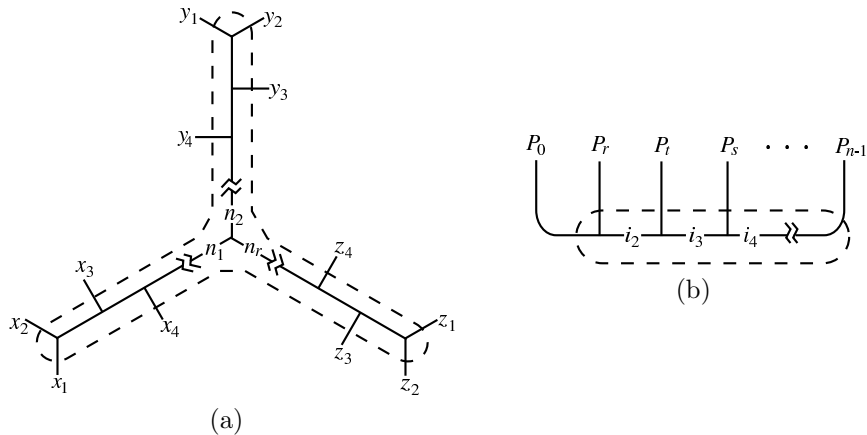


Figure 4: Two useful shapes for intertwiner bases. The first, in (a), is the “snowflake” basis. Its essential feature is that the edges of a given  $n$ -valent vertex are partitioned into three groups (denoted  $\{x_i\}$ ,  $\{y_i\}$ , and  $\{z_i\}$  in the diagram); each of the groups is then “collected” into a single edge (labelled  $n_1$ ,  $n_2$ , and  $n_r$ ); and finally, these three collecting edges form a trivalent vertex at the core of the vertex. The second basis, in (b), is the “comb” basis; in it, all the edges are lined up along a central “spine” of intertwiner edges (labelled  $i_2$ ,  $i_3$ ,  $i_4 \dots$  in the diagram.)

arbitrary shape into any other shape we wish. Two such useful shapes are the “snowflake” and “comb” bases, depicted in Figure 4.

The second such transformation is illustrated in Figure 5. This transformation allows us to switch the order of two adjacent edges along a branch of the intertwiner, while leaving the other branches in their original order. Thus, any order of edges is possible along a given intertwiner shape; this fact will become vitally important to us in our discussion of the volume operator in Section 3.5.4.

### 3.3 Spin Networks & Angular Momentum Coupling

The trivalent vertex rules introduced in Section 3.1, and their generalized versions in (3.17) and (3.18), are not entirely transparent. However, a simple analogy exists which may make these rules more intuitive to the reader; there is a striking parallel between the coupling of angular momenta in quantum mechanics and spin networks.<sup>11</sup>

To draw this parallel, let us relabel all the edges of a given trivalent vertex with half their original values. In other words, an edge with colour 1 becomes an edge with colour  $\frac{1}{2}$ ; an edge with colour 2 becomes an edge with colour 1; and in general, an edge with colour  $i$  is reassigned a new colour  $i' = i/2$ . In terms

<sup>11</sup>Indeed, this similarity is the very source of the name “spin” networks.

$$\begin{aligned}
& \cdots -i_1 \overbrace{\quad}^{i_2} \quad -i_3 \quad -i_4 \cdots \\
& \quad \quad \quad \begin{array}{c} | \\ a_1 \\ | \\ a_2 \\ | \\ a_3 \end{array} \\
& = \sum_{j_2} \left\{ \begin{array}{ccc} a_1 & i_1 & j_2 \\ i_3 & a_2 & i_2 \end{array} \right\} \begin{array}{c} \cdots -i_1 \quad -i_3 \quad -i_4 \cdots \\ \quad \quad \quad \begin{array}{c} | \\ j_2 \\ \diagdown a_1 \quad \diagup a_2 \\ | \\ a_3 \end{array} \end{array} \\
& = \sum_{j_2} \left\{ \begin{array}{ccc} a_1 & i_1 & j_2 \\ i_3 & a_2 & i_2 \end{array} \right\} \lambda_{j_2}^{a_1 a_2} \begin{array}{c} \cdots -i_1 \quad -i_3 \quad -i_4 \cdots \\ \quad \quad \quad \begin{array}{c} | \\ j_2 \\ \diagup a_2 \quad \diagdown a_1 \\ | \\ a_3 \end{array} \end{array} \\
& = \sum_{j_2} \sum_{k_2} \left\{ \begin{array}{ccc} a_1 & i_1 & j_2 \\ i_3 & a_2 & i_2 \end{array} \right\} \lambda_{j_2}^{a_1 a_2} \left\{ \begin{array}{ccc} a_1 & a_2 & k_2 \\ i_1 & i_3 & j_2 \end{array} \right\} \begin{array}{c} \cdots -i_1 \quad -k_2 \quad -i_3 \quad -i_4 \cdots \\ \quad \quad \quad \begin{array}{c} | \\ a_3 \\ | \\ a_1 \\ | \\ a_3 \end{array} \end{array}
\end{aligned}$$

Figure 5: The “swap transformation”, in which two edges along an internal spine are switched. Note that in the third step we have applied the lambda move (B.6) to the vertex indicated in the previous step.

of these half-integer edge colours, the constraints that the edges must satisfy become:

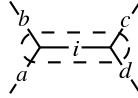
$$a' + b' \geq c' \quad b' + c' \geq a' \quad c' + a' \geq b' \quad (\text{as before}) \quad (3.19)$$

$$a' + b' + c' \text{ is an integer} \quad (3.20)$$

As it happens, these rules are exactly the same as those for the coupling of particles with angular momentum. If we wish to couple together a spin- $a'$  and a spin- $b'$  particle to form a spin- $c'$  particle, the three spins  $a'$ ,  $b'$ , and  $c'$  must satisfy the triangle inequalities, as in (3.19); as well, the sum of the three spins must be an integer, as in (3.20).

As a concrete example of this parallel, consider a trivalent vertex with an edge with colour 1, an edge with colour 2, and the third edge colour  $m$  as yet undetermined. According to the vertex rules, we must have  $m = 1$  or  $m = 3$ ; any value less than 1 or greater than 3 would violate the triangle inequalities, and a value of 2 would violate the evenness requirement. The angular momentum coupling scheme which correspond to this vertex would be the coupling of a spin- $\frac{1}{2}$  particle to a spin-1 particle; according to the rules of such couplings, the resulting spin must be either  $\frac{1}{2}$  or  $\frac{3}{2}$ .

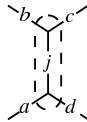
We can draw a similar parallel between 4-valent vertices and three-particle coupling schemes. Consider again the following vertex:



Suppose  $a = 2$ ,  $b = 3$ , and  $c = 3$ . According to the vertex rules, this means that  $d$  must have a value of 0, 2, 4, 6, or 8. Similarly, if we couple together

one spin-1 particle and two spin- $\frac{3}{2}$  particles, the resulting total spin can be 0, 1, 2, 3, or 4. In fact, this rule holds for a general vertex with valence  $n$ , with incoming spins  $a_1, a_2, \dots, a_n$ ; such a vertex can be translated into a coupling scheme of  $n-1$  spins  $a'_1, a'_2, \dots, a'_{n-1}$  to yield a total spin of  $a'_n$ , where  $a'_i = a_i/2$  for  $i = 1, 2, \dots, n$ .

The reader may be asking at this point whether any analogy for the internal edges of a higher-valence vertex exists in angular momentum coupling schemes. In fact, such an analogy does exist. In the above diagram, we can view the total coupling as happening in two stages: first particle  $a$  and particle  $b$  couple to form a particle  $i$ , then particle  $i$  and particle  $c$  couple to form particle  $d$ . Of course, the coupling does not necessarily have to take place in this order. For instance, we could equally well have coupled particles  $b$  and  $c$  together first, to form a particle  $j$ , and then couple particle  $j$  to particle  $a$  to form particle  $d$ ; this is an equally valid way to couple the three particles together. Similarly, we can represent a vertex with edges  $a, b, c$ , and  $d$  in a second form:



The parallel between the intertwiner of this vertex and this second angular momentum coupling scheme is evident.

Finally, we note the following: In angular momentum coupling, we translate between these two coupling schemes (i.e. particle  $i$  vs. particle  $j$ ) using the *Wigner 6-j symbols*; in spin networks, we use the recoupling theorem and the *Kauffman-Lins 6-j symbols* to translate between intertwiners. Given the above parallels, it should not surprise us to learn that the Wigner and the Kauffman-Lins 6-j symbols are related; for more details, see Appendix C.

### 3.4 Spin Networks & Holonomies

The reader may be wondering at this point what, exactly, the connection between the spin networks we have just described and the holonomies described in Section 2 is. To answer this question, consider a simple network in space, shown in Figure 6, along with three paths (or sets of paths) in this network. To label these paths, we must introduce a few concepts. We define the composition of two paths to be the path obtained by traversing the two paths in order; for example, the path  $\alpha \circ \gamma$  is obtained by going around  $\alpha$ , then going along  $\gamma$ . We also introduce the concept of inverses of a path, which we define (intuitively) to be the same path traversed in the opposite direction; for example, the path  $\alpha \circ \gamma \circ \gamma^{-1}$  is obtained by traversing  $\alpha$  forwards, then  $\gamma$  forwards, then  $\gamma$  backwards (i.e. retracing our steps along  $\gamma$ ). Using this notation, the three paths can be labelled  $\alpha \cup \beta$ ,  $\alpha \circ \gamma \circ \beta \circ \gamma^{-1}$ , and  $\alpha \circ \gamma \circ \beta^{-1} \circ \gamma^{-1}$ .

One might think that the state vectors corresponding to these three loops would be independent; unfortunately, this is not the case. Recall that each path

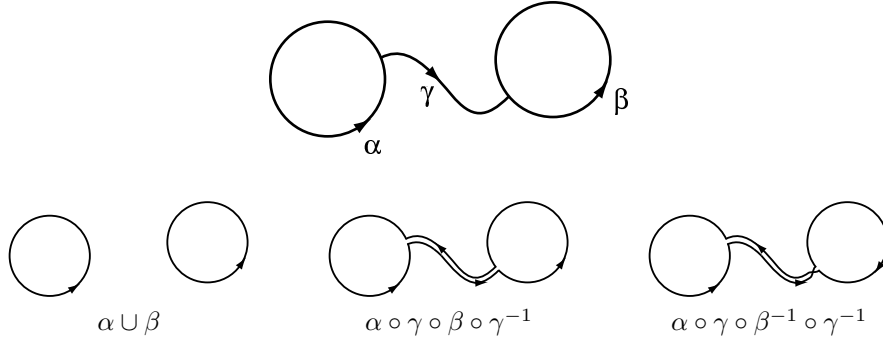


Figure 6: A simple network in space, and three paths (or sets of paths) within it.

in the manifold  $\Sigma$  has a matrix from the group  $SU(2)$  associated with it. Given any two matrices  $A, B \in SU(2)$ , their traces satisfy the following identity:

$$\text{Tr}(A)\text{Tr}(B) - \text{Tr}(AB) - \text{Tr}(AB^{-1}) = 0 \quad (3.21)$$

Since this linear combination is equal to zero, the quantum states corresponding to each one of these terms satisfy an analogous identity:

$$\langle \alpha \cup \beta | - \langle \alpha \circ \gamma \circ \beta \circ \gamma^{-1} | - \langle \alpha \circ \gamma \circ \beta^{-1} \circ \gamma^{-1} | = 0. \quad (3.22)$$

Hence, these three states are linearly dependent.

For a fairly simple network (such as the one just described), it might be possible to keep track of all the identities satisfied by loops in the network. However, for a more complicated network the number of these identities skyrockets; it would be nice, then, if we could find a way to avoid these identities altogether.

As the reader may have guessed by now, spin networks allow us to do this. Consider the states

$$\begin{aligned} \langle \alpha \cup \beta | &= \langle \alpha \circ \gamma \circ \beta \circ \gamma^{-1} | + \langle \alpha \circ \gamma \circ \beta^{-1} \circ \gamma^{-1} | \quad \text{and} \\ \langle \alpha \circ \gamma \circ \beta \circ \gamma^{-1} | &- \langle \alpha \circ \gamma \circ \beta^{-1} \circ \gamma^{-1} |. \end{aligned} \quad (3.23)$$

These two states are independent of each other, and (just as importantly) span the entire space of loops on this network — any loop or set of loops on this network can be written as a linear combination of these states (using the identity in 3.22 if necessary.) However, the second one of these states can be rewritten

in a more familiar form:

$$\begin{aligned}
 & \langle \alpha \circ \gamma \circ \beta \circ \gamma^{-1} | - \langle \alpha \circ \gamma \circ \beta^{-1} \circ \gamma^{-1} | \\
 &= \left\langle \begin{array}{c} \text{Two circles connected by a wavy edge with arrows pointing right.} \end{array} \right| - \left\langle \begin{array}{c} \text{Two circles connected by a wavy edge with arrows pointing left.} \end{array} \right| \\
 &= \left\langle \begin{array}{c} \text{Two circles connected by a wavy edge with arrows pointing right.} \\ \text{The left circle has a small '1' at the bottom, and the right circle has a small '1' at the top.} \end{array} \right|
 \end{aligned}$$

Hence, given a network in  $\Sigma$ , the introduction of spins on the edges eliminates the identities that might otherwise be present. In this way, spin networks represent a basis for the states of loop quantum gravity.

### 3.5 Operators on Spin Networks

We have now defined our quantum states in terms of spin networks. A successful theory of quantum gravity should be able to make predictions about “spatial observables” such as area, volume, and angle — geometric quantities that we would normally be able to measure on a classical manifold. As in any quantum theory, this is done by Hermitian operators which act on the spin networks and return eigenvalues corresponding to observable quantities. However, it is not at all clear what these operators should be.

We will describe the actions of four operators — angular momentum, area, angle, and volume — in varying degrees of detail. In general, however, the construction of quantum operators from first principles is a complex process; hence, we will not try to do so in this work. The reader wanting further details as to the construction of these operators is referred to the derivations in [10] (for angular momentum), [13, 14] (for area), [15] (for angle), and [12] (for volume).

#### 3.5.1 Angular Momentum Operators

One of our primary concerns in this thesis will be to describe the angles associated with a given vertex; to define angles, however, we need to be able to associate a direction (i.e. a vector) with an edge or a group of edges. In Penrose’s original formulation of spin networks, the labels on the edges actually refer to angular momenta “carried” by the edges (see Section 3.3); hence, one of the most natural directions to associate with an edge is its angular momentum vector.

These angular momenta can be measured by the angular momentum operators, which act upon the edges. The angular momentum operators are expressed in terms of the Pauli spin matrices  $\sigma_i$ :

$$\sigma_1 = \begin{pmatrix} 0 & 1 \\ 1 & 0 \end{pmatrix}, \quad \sigma_2 = \begin{pmatrix} 0 & -i \\ i & 0 \end{pmatrix}, \quad \sigma_3 = \begin{pmatrix} 1 & 0 \\ 0 & -1 \end{pmatrix} \quad (3.24)$$

The operators themselves are then defined in terms of these matrices “grasping” the edges:

$$\hat{\sigma}_i = \left[ \sigma_i \right] \text{---} 2 \text{---} \square \quad (3.25)$$

where the small square at the end indicates that this operator will “grasp” the edge. If the strand in question happens to be a multiple strand, then this grasping will apply to each strand in it; hence, we can show that a 2-edge grasping an  $m$ -edge is equivalent to  $m$  times a trivalent vertex with edges  $m$ ,  $m$ , and 2:

$$\text{---} 2 \text{---} \square \text{---} m = m \text{---} 2 \text{---} \square \text{---} m \quad (3.26)$$

Using this, we can define angular momentum operators  $\hat{J}_i = \frac{\hbar}{2}\hat{\sigma}_i$  which act on the edges; these operators have the usual properties of angular momentum operators.<sup>12</sup> As we might expect, we can also construct the  $\hat{J}^2$  operator. This is equal to the sum of the squares of the three  $\hat{J}_i$  operators, i.e.  $\hat{J}^2 = \hat{J}_1^2 + \hat{J}_2^2 + \hat{J}_3^2$ . We can use diagrammatics and graspings to find the eigenvalues of this operator; however, it is much simpler to note that the Pauli matrices have the following identity, which is easily expressible in terms of spin networks:

$$\frac{1}{2} \sum_{i=1}^3 \sigma_{iA}^B \sigma_{iC}^D = \frac{1}{2} (\epsilon_{AC} \epsilon^{BD} - \delta_A^D \delta_C^B) = \frac{1}{2} \left( \begin{array}{c} \text{B} \quad \text{D} \\ \text{---} \quad \text{---} \\ \text{A} \quad \text{C} \end{array} - \begin{array}{c} \text{B} \quad \text{D} \\ \text{---} \quad \text{---} \\ \text{A} \quad \text{C} \end{array} \right) = \begin{array}{c} \text{B} \quad \text{D} \\ \text{---} \quad \text{---} \\ \text{A} \quad \text{C} \end{array} \quad (3.27)$$

Hence, instead of expressing  $\hat{J}^2$  in terms of the sum of three operators, we can express it very simply in diagrammatic form:

$$\hat{J}^2 = \frac{\hbar^2}{2} \begin{array}{c} \square \\ \text{---} \\ \square \end{array} \quad (3.28)$$

where we now grasp with two ‘‘hands’’ on the edge in question. Using the ‘‘bubble’’ identity (B.5), this becomes

$$\begin{aligned} \hat{J}^2 \Big|_m &= \frac{\hbar^2}{2} m^2 \begin{array}{c} \square \\ \text{---} \\ \square \end{array} \Big|_m \\ &= \frac{\hbar^2}{2} m^2 \frac{(-1)^m \theta(m, m, 2)}{m+1} \Big|_m \end{aligned}$$

Note that the factor of  $m^2$  in the first step comes from the two graspings of the 2-edge. If we apply the identity (B.3) to this equation, we get

$$\begin{aligned} \hat{J}^2 \Big|_m &= \frac{\hbar^2}{2} m^2 \frac{(-1)^m}{m+1} \frac{(-1)^{m+1} (m+2)(m+1)}{2m} \Big|_m \\ &= -\hbar^2 \frac{m(m+2)}{4} \Big|_m \end{aligned} \quad (3.29)$$

If we make the identification  $j = m/2$ , then the eigenvalues simplify to the easily recognizable form  $\hbar^2 j(j+1)$ .<sup>13</sup> This operator (and its eigenvalues) will become important in our discussion of the area and angle operators.



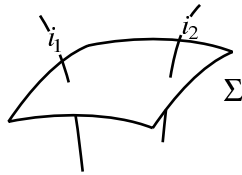


Figure 7: A surface  $\Sigma$  whose area we wish to find. The contribution to the area from the portion of the surface shown would be the sum of the contribution from each of the two edges  $i_1$  and  $i_2$  intersecting this portion.

### 3.5.2 The Area Operator

In the spin-network version of quantum gravity, the area operator is the simplest to define. If we have a closed surface  $\Sigma$  which intersects our spin network in  $N$  points, its area can be decomposed into a contribution from each of these intersections:

$$A[\Sigma] = \sum_{i=1}^N A_i \quad (3.30)$$

As it turns out, it is much easier to derive the action of the area-squared operator  $A_i^2$  than to directly find the action of the area operator; this action turns out to be the double grasping of a two-edge times the square of the Planck length  $l_0$ , defined in (1.1):

$$\hat{A}_i^2 = l_0^2 \begin{array}{c} \square \\ \curvearrowright \\ \square \end{array} \quad (3.31)$$

The reader will notice that we have already done the work to find the eigenvalues of this operator in the previous section; the result, from (3.29), is then

$$\hat{A}_i^2 \Big|_m = l_0^2 \frac{m(m+2)}{4} \Big|_m \quad (3.32)$$

The total area of  $\Sigma$  is then given by

$$A[\Sigma] = l_0 \sum_i \sqrt{\frac{m_i(m_i+2)}{4}} \quad (3.33)$$

where the summation of  $i$  is over all edges that intersect  $\Sigma$ , and  $m_i$  is the edge label of the edge  $i$ .

<sup>12</sup> The actual eigenvalues of the operators  $\hat{J}_i$  will not concern us here; however, it is worth noting that doing so requires (loosely speaking) giving orientations to the edges. Since this is not required in the spin-network formulation of quantum gravity, we will not go into it here.

<sup>13</sup> The reader will notice that the sign of this expression is incorrect. This stems from a difference between the properties of the “angular momentum” spin networks originally studied by Penrose and those used for quantum gravity.

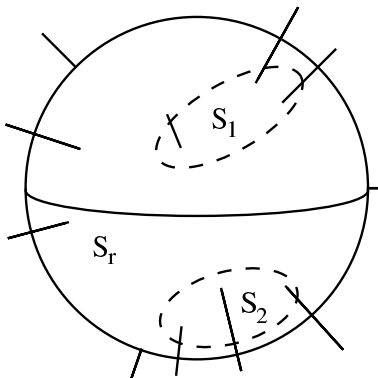


Figure 8: Partition of the edges surrounding a vertex into three groups  $S_1$ ,  $S_2$ , and  $S_3$ . (The vertex itself is inside the sphere.) The angle operator will return the angle between the patches  $S_1$  and  $S_2$ .

### 3.5.3 The Angle Operator

The angle operator acts on a vertex as follows: we can imagine a surface encompassing a vertex of arbitrary valence. We select two “patches” on the surface  $S_1$  and  $S_2$ , and call the remaining area of the surface  $S_r$  (as in Figure 8). This defines a partition of the edges into three groups corresponding to the three patches  $S_1$ ,  $S_2$ , and  $S_r$ . The intertwiner basis for this vertex is decomposed in such a way that all edges belonging to one group are “collected” into one internal edge; the three internal edges created in this way then join at a trivalent “core;” see Figure 9.<sup>14</sup> For future use, we will also define the quantities  $s_1$ ,  $s_2$ , and  $s_r$  as the sum of the labels of all the edges traversing  $S_1$ ,  $S_2$ , and  $S_r$ , respectively; similarly, we will define  $n_1$ ,  $n_2$ , and  $n_r$  as the internal labels of their respective collecting edges.

Although a rigorous derivation of the provenance of the angle operator is rather complicated, it is possible to gain an intuitive understanding as follows. The angle operator will measure the angle between the “bunches” of edges that traverse  $S_1$  and those that traverse  $S_2$ . The most “natural” direction that is associated with the edges traversing  $S_1$ ,  $S_2$ , and  $S_r$  is the angular momentum vectors associated with their internal edges (which we define as  $\vec{J}_1$ ,  $\vec{J}_2$ , and  $\vec{J}_r$  respectively). Classically, we would expect the angle between  $\vec{J}_1$  and  $\vec{J}_2$  to be given by

$$\cos \theta = \frac{\vec{J}_1 \cdot \vec{J}_2}{|\vec{J}_1| |\vec{J}_2|} \quad (3.34)$$

<sup>14</sup>Note that even if the internal structure of the intertwiner is not of this form for the partition we choose, it can be viewed as a superposition of such intertwiners (using the techniques stated in section 3.2.)

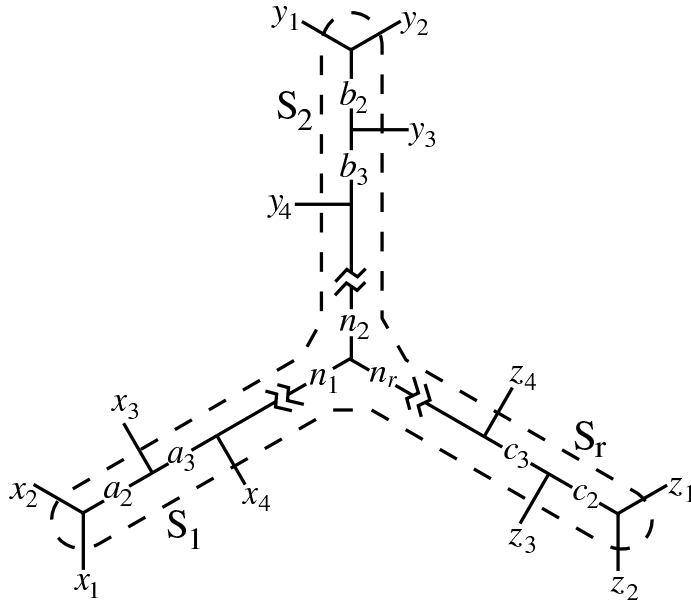


Figure 9: Internal decomposition of a vertex operated on by the angle operator; the dotted line denotes the boundary between external and internal edges. All of the edges  $x_1, x_2, \dots$  which intersect the surface  $S_1$  are “collected” into the internal edge labelled with  $n_1$ ; similarly, all the edges which intersect  $S_2$  are collected into the edge labelled  $n_2$ , and the edges which intersect  $S_r$  are collected into the edge labelled  $n_r$ . In the text, we denote  $s_1 = \sum x_i$ ,  $s_2 = \sum y_i$ , and  $s_r = \sum z_i$ .

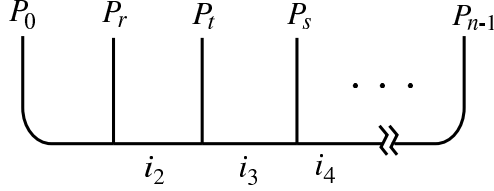


Figure 10: Internal decomposition of a vertex to be operated on by the volume operator. The external edges  $P_0, P_1, \dots, P_{n-1}$  are “lined up” along an internal “spine.” The edges  $i_2, i_3, \dots, i_{n-2}$  are internal.

However, since we don’t want a net angular momentum to be associated with a point in empty space, we require that

$$\vec{J}_1 + \vec{J}_2 + \vec{J}_r = 0. \quad (3.35)$$

Using this, we can put the quantity in (3.34) in terms of  $J^2$  operators:

$$\begin{aligned} (\vec{J}_r)^2 &= (\vec{J}_1 + \vec{J}_2)^2 \\ J_r^2 &= J_1^2 + J_2^2 + 2\vec{J}_1 \cdot \vec{J}_2 \\ \vec{J}_1 \cdot \vec{J}_2 &= \frac{1}{2} (J_r^2 - J_1^2 - J_2^2) \end{aligned} \quad (3.36)$$

The angle operator is then defined as

$$\hat{\theta} = \arccos \left( \frac{J_r^2 - J_1^2 - J_2^2}{2\sqrt{J_1^2}\sqrt{J_2^2}} \right) \quad (3.37)$$

Since we know the action of the  $J^2$  operators already, we can readily state the eigenvalues of the angle operator:

$$\theta = \arccos \left( \frac{n_r(n_r + 2) - n_1(n_1 + 2) - n_2(n_2 + 2)}{2\sqrt{n_1(n_1 + 2)}\sqrt{n_2(n_2 + 2)}} \right) \quad (3.38)$$

We note briefly that there are important philosophical considerations which arise from the discrete spectrum of this operator as it relates to diffeomorphism invariance. These considerations are discussed in Appendix D; we will not go into them here.

### 3.5.4 The Volume Operator

The volume operator also acts on a vertex. In this case, however, it is more convenient to use the basis pictured in Figure 10, where all the edges are lined up sequentially. As we did for the area operator, we will also find it easier to define the volume-squared operator (known as  $W$ ) first; the volume eigenvalues are then the square roots of the absolute values of the eigenvalues of  $W$ .

The action of  $W$  itself is rather complicated. For a vertex with  $n$  edges labelled  $\{P_0, P_1, \dots, P_{n-1}\}$ , we define an operator  $W_{[rst]}$  for each triad of edges such that  $0 \leq r < s < t \leq n-1$ . The action of  $W_{[rst]}$  consists of three 2-edges, joined at a trivalent intersection, which grasp edges  $r$ ,  $s$ , and  $t$  as follows:

$$\hat{W}_{[rst]} = 2 \left[ \begin{array}{c} \square \\ | \\ 2 \\ | \\ \square \end{array} \right] \quad (3.39)$$

$$\hat{W}_{[rst]} \left[ \begin{array}{c} P_0 \\ | \\ \vdots \\ | \\ P_r \\ | \\ \vdots \\ | \\ P_s \\ | \\ \vdots \\ | \\ P_t \\ | \\ \vdots \\ | \\ P_{n-1} \end{array} \right] = P_r P_s P_t \left[ \begin{array}{c} P_0 \\ | \\ \vdots \\ | \\ P_r \\ | \\ \vdots \\ | \\ P_s \\ | \\ \vdots \\ | \\ P_t \\ | \\ \vdots \\ | \\ P_{n-1} \end{array} \right] \quad (3.40)$$

Since the ‘‘comb’’ basis spans the space of all intertwiners, we can write the action of the  $W$  operator as sending the original vertex to a superposition of other vertices in the same basis:

$$\hat{W}_{[rst]} \left[ \begin{array}{c} P_0 \\ | \\ \vdots \\ | \\ P_r \\ | \\ \vdots \\ | \\ P_s \\ | \\ \vdots \\ | \\ P_t \\ | \\ \vdots \\ | \\ P_{n-1} \end{array} \right] = \sum_{k_2, \dots, k_{n-2}} W_{[rst] i_2, \dots, i_{n-2}}^{k_2, \dots, k_{n-2}} \left[ \begin{array}{c} P_0 \\ | \\ \vdots \\ | \\ k_2 \\ | \\ \vdots \\ | \\ k_3 \\ | \\ \vdots \\ | \\ k_4 \\ | \\ \vdots \\ | \\ P_{n-1} \end{array} \right] \quad (3.41)$$

This is essentially a matrix equation; the entries of the matrix are now indexed by the internal intertwiner edges. We can find these entries through extensive use of the identities in Section 3. This result was first found in [12]; the matrix entries turn out to be

$$\begin{aligned} W_{[rst] i_2, \dots, i_{n-2}}^{(n) k_2, \dots, k_{n-2}} = & \\ & -P_r P_s P_t \left\{ \begin{array}{c} k_2 \quad P_t \quad k_3 \\ i_2 \quad P_t \quad i_3 \\ 2 \quad 2 \quad 2 \end{array} \right\} \lambda_{k_2}^{i_2} \delta_{i_4}^{k_4} \dots \delta_{i_{n-2}}^{k_{n-2}} \\ & \times \frac{\text{Tet} \left[ \begin{array}{c} P_r \quad P_r \quad P_0 \\ k_2 \quad i_2 \quad 2 \end{array} \right] \text{Tet} \left[ \begin{array}{c} P_s \quad P_s \quad k_4 \\ k_3 \quad i_3 \quad 2 \end{array} \right] \Delta_{k_2} \Delta_{k_3}}{\theta(k_2, i_2, 2) \theta(k_3, i_3, 2) \theta(P_0, P_r, k_2) \theta(k_2, k_3, P_t) \theta(k_3, k_4, P_s)} \quad (3.42) \end{aligned}$$

This expression simplifies somewhat if we express it in terms of the Kauffman-Lins 6- $j$  symbols (see Appendix C):

$$\begin{aligned} W_{[rst] i_2, \dots, i_{n-2}}^{(n) k_2, \dots, k_{n-2}} = & -P_r P_s P_t \left\{ \begin{array}{c} k_2 \quad P_t \quad k_3 \\ i_2 \quad P_t \quad i_3 \\ 2 \quad 2 \quad 2 \end{array} \right\} \lambda_{k_2}^{i_2} \delta_{i_4}^{k_4} \dots \delta_{i_{n-2}}^{k_{n-2}} \\ & \times \frac{\left\{ \begin{array}{c} P_r \quad P_r \quad P_0 \\ k_2 \quad i_2 \quad 2 \end{array} \right\} \left\{ \begin{array}{c} P_s \quad P_s \quad k_4 \\ k_3 \quad i_3 \quad 2 \end{array} \right\}}{\theta(k_2, k_3, P_t)} \quad (3.43) \end{aligned}$$





## 4 The Angle Operator

Although the form of the angle and volume operators are known, many of their properties have not yet been examined. In this section and Section 5, we describe the results of original research done into the properties of these operators.

### 4.1 Spectrum of the Angle Operator

Recall from Section 3.5.3 that the eigenvalues of the angle operator are given by the formula

$$\theta = \arccos \left( \frac{j_r(j_r + 1) - j_1(j_1 + 1) - j_2(j_2 + 1)}{2\sqrt{j_1(j_1 + 1)j_2(j_2 + 1)}} \right). \quad (4.1)$$

We will find it more convenient to use the core edge colours  $n_1$ ,  $n_2$ , and  $n_r$  instead of their associated spins; in terms of these labels, the angle becomes

$$\theta = \arccos \left( \frac{n_r(n_r + 2) - n_1(n_1 + 2) - n_2(n_2 + 2)}{2\sqrt{n_1(n_1 + 2)n_2(n_2 + 2)}} \right), \quad (4.2)$$

where

$$j_x = \frac{n_x}{2}.$$

Note that the quantities  $n_1$ ,  $n_2$ , and  $n_r$  are the intertwiner edges that “collect” the spins from each of the three surface patches; they are related to the total edge flux intersecting each patch by the relations

$$n_1 \leq s_1, n_2 \leq s_2, \text{ and } n_r \leq s_r \quad (4.3)$$

where  $s_1$ ,  $s_2$ , and  $s_r$  are the respective surface fluxes.

The easiest way to visualize the angle spectrum is to plot its possible eigenvalues versus the total core spin (defined as  $n_T = n_r + n_1 + n_2$ ). Such a plot is shown in Figure 11. This plot shows two interesting features. First, we note the existence of fan-like structures, consisting of several sequences splitting off from a sort of “spine”. (Such a structure has been isolated in Figure 12. Second, and perhaps more importantly, there seem to be very few eigenvalues corresponding to small angles. We will deal with the latter of these phenomena first.

To obtain a small angle, we want the argument of the inverse cosine in (4.2) to be as close to 1 as possible:

$$Q \equiv \frac{n_r(n_r + 2) - n_1(n_1 + 2) - n_2(n_2 + 2)}{2\sqrt{n_1(n_1 + 2)n_2(n_2 + 2)}} \quad (4.4)$$

However, the internal edge spins are subject to the triangle inequalities:

$$2n_1, 2n_2, 2n_r \leq n_1 + n_2 + n_r$$



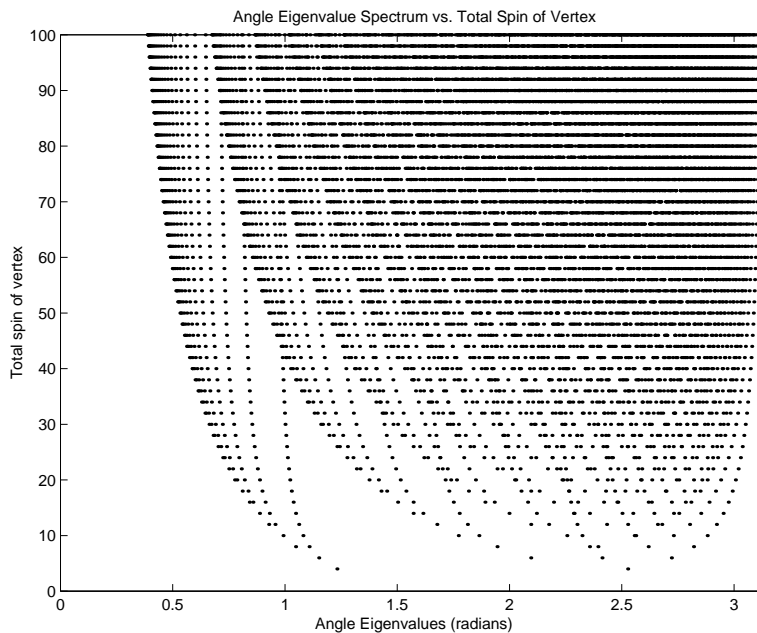


Figure 11: Angle operator spectrum for increasing total vertex spin.

To maximize  $Q$ , then, we wish to maximize its numerator and minimize its denominator while simultaneously respecting the triangle inequalities. This occurs when

$$n_r = \frac{n_T}{2} \text{ and } n_1 = n_2 \approx \frac{n_T}{4} \quad (4.5)$$

where  $n_T$  is as defined above.<sup>15</sup> At these values of  $n_1$ ,  $n_2$ , and  $n_r$ , the argument of the inverse cosine then reduces to

$$Q = \frac{n_T}{n_T + 8}. \quad (4.6)$$

For any angle  $\epsilon$ , then, we have the relation

$$\epsilon \geq \arccos\left(\frac{n_T}{n_T + 8}\right)$$

<sup>15</sup> Note that while the value for  $n_r$  is exact, the values of  $n_1$  and  $n_2$  are only approximate; this is because  $n_T$  must be even, but may not necessarily be divisible by 4, and because  $n_1$ ,  $n_2$ , and  $n_r$  must be integers. However, for large values of  $n_T$ , the values of  $n_1$  and  $n_2$  that maximize  $Q$  will approach  $n_T/4$ .

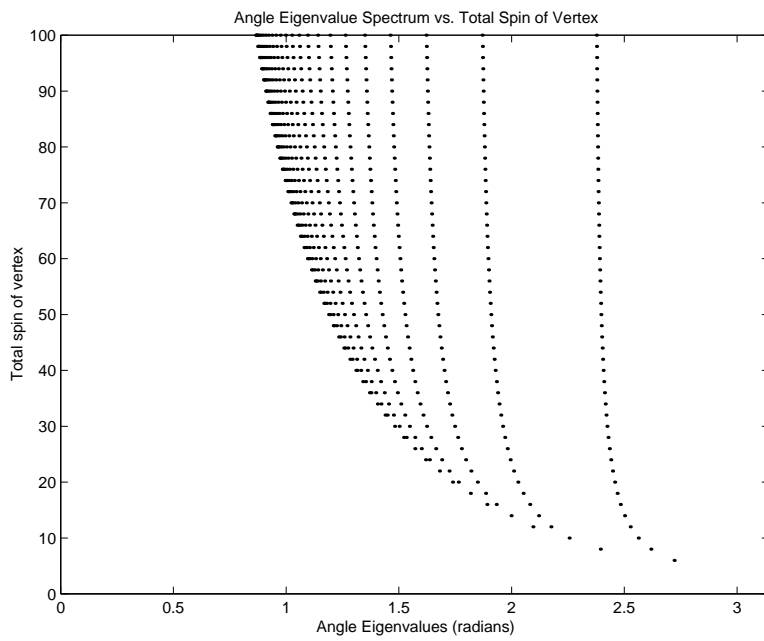


Figure 12: One of the fan-like structures that develop as  $m$  increases. This particular fan consists of sequences for which  $n_1 + n_2 - n_r = 4$ .

For small  $\epsilon$ ,  $\cos x$  is a uniformly decreasing function; hence, for  $\epsilon \ll 1$ , we have

$$\begin{aligned} \cos \epsilon &\leq \frac{n_T}{n_T + 8} \\ 1 - \frac{\epsilon^2}{2} &\leq 1 - \frac{8}{n_T + 8} \\ \epsilon &\geq \frac{4}{\sqrt{n_T + 8}} \end{aligned} \tag{4.7}$$

Hence, for large values of  $n_T$ , the minimum possible angle between two patches is roughly proportional to  $n_T^{-1/2}$ . Moreover, we note that if  $s_R > s_1 + s_2$ , then  $n_T \leq 2(s_1 + s_2)$ ; this implies that for a “macroscopic” vertex, where  $s_r \gg s_1, s_2$ , the minimum observable angle depends only on the edge flux through the patches whose angular separation we are measuring.

The first observation (i.e. the fan-like structures) is somewhat harder to quantify. A bit of investigation shows that the “feathers” of the fans in Figure 12 are sequences of the form

$$n_r = m, n_1 = m - r, \text{ and } n_2 = q,$$

where  $m$  varies and  $r$  and  $q$  are constant. From the triangle inequalities, we find that

$$|r| \leq q \text{ and } r + q \text{ is even.}$$

The angles associated with such a vertex are given by

$$\cos \theta = \frac{2mr - r^2 - q^2 - 2q}{2\sqrt{q(q+2)}(m^2 - 2m(r-1) + r(r-2))}, \tag{4.8}$$

and for  $r, q \ll m$ , the sequences will approach the value

$$\cos \theta = \frac{r}{\sqrt{q(q+2)}} \tag{4.9}$$

It is natural to ask whether any real number in the interval  $[-1, 1]$  is arbitrarily close to a number of this form; if this were true, then it would follow that any angle could be approximated by a vertex with sufficiently large internal spin. It turns out that this is true:

**Lemma 1** *For any real number  $x \in [-1, 1]$  and any  $\epsilon > 0$ , there exist integers  $q$  and  $r$  such that*

$$\left| x - \frac{r}{\sqrt{q(q+2)}} \right| < \epsilon.$$

**Proof:** Choose integers  $b$  and  $c$  such that

$$\left| x - \frac{b}{c} \right| < \frac{\epsilon}{2};$$

this can be done because the rational numbers are dense in the reals. Further, choose another integer  $n$  such that

$$\left| \frac{b}{c} \left( 1 - \frac{1}{\sqrt{1 + 2/nc}} \right) \right| < \frac{\epsilon}{2};$$

this can be done since the quantity on the left-hand side of the equation can be viewed as a function which approaches 0 as  $n \rightarrow \infty$ . So, if we set  $r = nb$  and  $q = nc$ , we have

$$\begin{aligned} \left| x - \frac{r}{\sqrt{q(q+2)}} \right| &= \left| x - \frac{nb}{\sqrt{nc(nc+2)}} \right| \\ &= \left| x - \frac{b}{c} \left( \frac{1}{\sqrt{1 + 2/nc}} \right) \right| \\ &\leq \left| x - \frac{b}{c} \right| + \left| \frac{b}{c} \left( 1 - \frac{1}{\sqrt{1 + 2/nc}} \right) \right| \\ &< \epsilon. \end{aligned}$$

Hence, we can approximate any angle  $\theta$  to arbitrary accuracy as long as we have a vertex of sufficiently high spin. We note that this is merely a confirmation of Moussouris' spin geometry theorem [18].

It is important to note, however, that while this proof shows the existence of vertices which yield any angle to arbitrary accuracy, it does nothing to associate a minimum total spin to this angle and accuracy. As it turns out, this task would be fairly difficult to accomplish by using these sequences. If we expand the expression in (4.8) to first order in  $m^{-1}$ , we end up with

$$\begin{aligned} \cos \theta &= \frac{1}{2\sqrt{q(q+2)}} (2mr - r^2 - q^2 - 2q)(m^2 - 2m(r-1) + r(r-2))^{-1/2} \\ &= \frac{1}{2m\sqrt{q(q+2)}} (2mr - r^2 - q^2 - 2q) \left( 1 + \frac{r-1}{m} \dots \right) \\ &\approx \frac{r}{\sqrt{q(q+2)}} \left( 1 + \frac{r-1}{m} \right) - \frac{r^2 + q^2 + 2q}{2m\sqrt{q(q+2)}} \\ &= \frac{r}{\sqrt{q(q+2)}} + \frac{1}{m} \frac{r(r-2) + q(q+2)}{2\sqrt{q(q+2)}} \end{aligned} \quad (4.10)$$

We see that in general the rapidity with which this sequence approaches its limit is very difficult to obtain: it depends non-trivially on the choice of  $r$  and  $q$ , which in turn depend non-trivially on the angle we wish to approximate and the accuracy to which we wish to approximate it.

In the special case where  $x$  can actually be written in the form  $r/\sqrt{q(q+2)}$ , however, it is fairly simple to determine the minimum spin required: simply plug  $r$  and  $q$  into the second term of (4.10) and find the minimum  $m$  that reduces

this term below the desired accuracy. Given this fact, the natural question to ask is whether any real number  $x$  can be written in this form. Unfortunately, this is not the case: any number of the form  $r/\sqrt{q(q+2)}$  is algebraic, so if  $x$  is transcendental it cannot be written in this form. Let us examine a case that is even more specialized: suppose  $x$  is of the form  $\sqrt{a/b}$ , where  $a$  and  $b$  are integers. We wish to find integer solutions to the equation

$$\frac{a}{b} = \frac{r^2}{q^2 + 2q},$$

which is equivalent to the second-order Diophantine equation (in  $q$  and  $r$ )

$$aq^2 + 2aq - br^2 = 0 \tag{4.11}$$

If we make the substitution  $p = q + 1$ , this equation takes on the form

$$ap^2 - br^2 - a = 0 \tag{4.12}$$

which has the (trivial) solution  $p = 1, r = 0$ . As it happens, there are recursion relations for Diophantine equations of this sort [19]; if we know one solution to a given equation, we can find other solutions using these relations. In this case, if there exist integer solutions  $u$  and  $v$  to the equation

$$u^2 - abv^2 = 1, \tag{4.13}$$

then  $p = u, r = av$  is a solution to (4.12):

$$au^2 - ba^2v^2 - a = a(u^2 - abv^2 - 1) = 0. \tag{4.14}$$

Equation (4.13) is known as a *Pell equation*; it has solutions when  $ab$  is not a perfect square.<sup>16</sup> However, the solutions are not always small, even for fairly small values of  $a$  and  $b$ . For example, if  $a = 1$  and  $b = 61$ , the smallest non-trivial solution to (4.11) is:

$$r = 226153980, q = 1766319050.$$

Also, solutions to (4.13) are found by the expansion of  $\sqrt{ab}$  in a continued fraction, i.e. an expression of the form

$$\sqrt{ab} = a_0 + \frac{1}{a_1 + \frac{1}{a_2 + \dots}}$$

Since the coefficients  $\{a_0, a_1, a_2, \dots\}$  vary widely depending on the choice of  $ab$ , so do the solutions.<sup>17</sup> Hence, we are forced to conclude that finding any angle  $\theta$  to an arbitrary accuracy  $\epsilon$  using this “fan” method is possible, but the solutions are difficult to find and have an extremely complicated dependence on  $\theta$  and  $\epsilon$ .

<sup>16</sup> Note that when  $ab$  is a perfect square,  $\sqrt{a/b} = a/\sqrt{ab}$  is rational.

<sup>17</sup>How these continued fractions relate to the solutions of the Pell equation is a fascinating subject which is, unfortunately, outside the scope of this piece. The interested reader is referred to Chrystal [20].

## 4.2 Mean Angular Resolution

Despite the difficulties in approximating a specific angle to arbitrary accuracy, it is possible to get an idea of the average separation between angles over the interval  $[0, \pi]$ . There are two ways to look at the mean angular separation. The simplest way of finding the “angular resolution” for a given vertex is to note that an  $n$ -valent vertex has  $n-2$  trivalent vertices in its intertwiner. Since each one of these internal vertices can be looked at as a “core” vertex, we can conclude that such a vertex has at most  $3(n-2)$  possible eigenvalues for the angle operator (the factor of three comes from regarding each of the three edges at each vertex as the  $n_r$  edge.) We define the mean angular resolution  $\delta$  to be the average separation between each possible angle and the next greatest possible angle; in other words,  $\delta$  is the average width of a “gap” between angles in the interval  $[0, \pi]$ . Since the  $3n-6$  eigenvalues associated with the vertex divide the interval into  $3n-5$  gaps, we conclude that the mean angular separation between the eigenvalues of the angle operator for an  $n$ -valent vertex is

$$\delta = \frac{\text{total of all gaps}}{\text{number of gaps}} = \frac{\pi}{3n-5} \quad (4.15)$$

However, this method does not take into account the fact that internal vertices may yield the same angles. For example, the internal vertices of a 4-valent vertex with all edges the same colour are identical; hence, when each of these internal vertices is treated as the core vertex by their respective angle operators, there will only be 2 possible angles instead of the expected 6. Since this degeneracy depends on the internal structure of the vertex, it is impossible to say much about it in general; the best we can do is to modify (4.15) to read

$$\delta \geq \frac{\pi}{3n-5} \quad (4.16)$$

This method, while legitimate, is somewhat limited: it only examines the separation between the eigenvalues of the angle operators that have a given vertex as their eigenstate. However, other angle measurements are possible for a given vertex. For example, if we measure the angle between two edges that do not immediately intersect in the vertex’s intertwiner, this measurement will not always yield a definite eigenvalue; instead, there will be an expectation value associated with this measurement. The question then becomes: for a given vertex, can we find the total number of possible expectation values for all possible measurements?

We note that given any vertex, we can partition its edges into three groups (one for  $S_1$ , one for  $S_2$ , and one for  $S_r$ .) If we switch basis to the “snowflake” basis, we will generally obtain a superposition of edges of this form; however, for a given superposition (corresponding to our original vertex) and a given partition, we will find a single expectation value. Hence, for a given vertex, the number of expectation values for the angle operator is equal to the number of partitions of its edges into three distinct groups.

Finding this number for a vertex with an arbitrary number of edges with arbitrary colours, however, is another question entirely. We note that the possible range of colours for the collecting edge is not dependent on the order of the edges along the branch; hence, the number of distinct partitions is given by

$$\mathcal{N} = \prod_{i=1}^{\infty} B(q_i), \quad (4.17)$$

where  $q_i$  is the number of edges with colour  $i$ , and  $B(n)$  is the number of distinct ways of partitioning  $n$  into three distinct bins (one bin for each branch).<sup>18</sup> Elementary combinatorics tells us that the number of ways to do this is

$$B(n) = \binom{(n+3)-1}{n} = \frac{(n+1)(n+2)}{2} \quad (4.18)$$

However, we must divide the overall product by two, since exchange of the sets corresponding to the  $n_1$  branch and the  $n_2$  branch yields the same angle. Thus, the maximum number of possible expectation values for a given vertex is

$$\mathcal{N} = \frac{1}{2} \prod_{i=1}^{\infty} \frac{(q_i+1)(q_i+2)}{2}. \quad (4.19)$$

In the case where all the edges have the same colour, this formula reduces to<sup>19</sup>

$$\mathcal{N} = \frac{(n+1)(n+2)}{4} \quad (4.20)$$

and the mean angular resolution (between expectation values) is given by

$$\delta \geq \frac{4\pi}{n^2 + 3n + 6} \quad (4.21)$$

---

<sup>18</sup> One might still wonder whether the expectation value of the operator could somehow depend on the order of the valent edges along the branches. To show that it does not, let us consider two states

$$|\psi_1\rangle = \sum_i a_i |n_1, n_2, n_r, \alpha_i\rangle \quad \text{and} \quad |\psi_2\rangle = \sum_i b_i |n_1, n_2, n_r, \beta_i\rangle$$

where  $n_1, n_2, n_r$  are the collecting edges, and  $\alpha_i$  and  $\beta_i$  are all other indices that can vary within the  $n_1, n_2, n_r$  subspace. (Note that the  $\alpha$  indices and the  $\beta$  indices are not necessarily in the same basis, but both bases span the  $n_1, n_2, n_r$  subspace.) The expectation values for each of these states are then

$$\langle \psi_1 | \theta | \psi_1 \rangle = f(n_1, n_2, n_r) \sum_i |a_i|^2 \quad \text{and} \quad \langle \psi_2 | \theta | \psi_2 \rangle = f(n_1, n_2, n_r) \sum_i |b_i|^2$$

where  $f(n_1, n_2, n_r)$  is the function of  $n_1, n_2, n_r$  given in (4.2). Since application of the recoupling theorem is a unitary basis transformation,  $\sum_i |a_i|^2 = \sum_i |b_i|^2$ ; hence, the expectation values of both states are the same.

<sup>19</sup>In general, we will call a vertex whose valent edge colours are all the same a *monochromatic* vertex; we will also refer to a monochromatic vertex whose edges are a specific color as a monochromatic vertex with edge colour  $m$ , or sometimes as an  $m$ -chromatic vertex.

where we have again used an inequality because of possible angle degeneracies.

It is important not to confuse the “mean angular resolution” as we have defined it with the average distance from a point in the interval  $[0, \pi]$  to the nearest angle (averaged over this interval). The quantity  $\delta$  that we have found allows us to get an idea of how tightly, on average, the eigenvalues of the angle operator for a given vertex are spaced. To find this other value (which, if found, would help us to estimate the level to which an arbitrary angle can be approximated) would

$$\langle \Delta \rangle = \sum_{\text{all gaps}} \left( \begin{array}{c} \text{prob. of being} \\ \text{located in the gap} \end{array} \right) \left( \begin{array}{c} \text{mean separation from} \\ \text{either end of gap} \end{array} \right) \quad (4.22)$$

This is equivalent to the expression

$$\langle \Delta \rangle = \sum_a \frac{w_a^2}{4\pi} \quad (4.23)$$

where  $w_a$  is the width of the gap  $a$ . This expression depends heavily on the precise location of the eigenvalues in the interval  $[0, \pi]$ , and is therefore difficult to compute analytically.

### 4.3 Angle Distribution

In the classical continuum model of space, the distribution of solid angles is proportional to  $\sin \theta$ :

$$\mathcal{P}(\theta) d\theta = \sin \theta d\theta \quad (4.24)$$

If our quantized angle operator is to be of any physical worth, it must reproduce this distribution in some “classical limit.” To find out whether this is so, we must examine not only the location of possible eigenvalues in the interval  $[0, \pi]$  (as we have in the past two sections), but also the likelihood with which these angles occur. Due to the complexity of this problem, we will consider only the simplest possible case which could still conceivably have a classical limit: that of an  $n$ -valent monochromatic vertex with edge colour 1.

We note that every vertex can be transformed into the snowflake basis by repeated application of the recoupling theorem. If we characterize these states by the internal spins  $a$ ,  $b$ , and  $c$ , this fact can be written algebraically as

$$|\psi\rangle = \sum_{a,b,c} C_{abc} |a_1, a_2, \dots, b_1, b_2, \dots, c_1, c_2, \dots\rangle \quad (4.25)$$

where  $a$ ,  $b$ , and  $c$  (without index) denote the sets  $\{a_1, a_2, \dots, a_i\}$ ,  $\{b_1, b_2, \dots, b_j\}$ , and  $\{c_1, c_2, \dots, c_k\}$  respectively. The most difficult part of this formula to analyze for arbitrary  $n$  is the coefficients  $C_{abc}$ ; finding these for a specific internal intertwiner structure could be done, although such a calculation would be mind-bogglingly tedious. For a random vertex, however, we do not know the exact



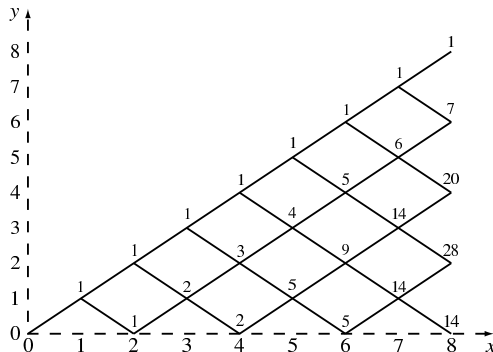


Figure 13: The lattice in the  $x$ - $y$  plane. The numbers above each intersection correspond to the number of paths from the origin to that intersection.

internal structure *a priori*; hence, there is no reason to assume that any given intertwiner is preferred. We will therefore assume that all intertwiners are equally likely. With this simplification in mind, we can conclude that the probability of measuring the angle associated with an intertwiner core  $n_1, n_2, n_r$  is given by

$$\mathcal{P}(\theta(n_1, n_2, n_r)) \propto \left( \frac{\text{number of intertwiners}}{\text{with core } n_1, n_2, n_r} \right) \quad (4.26)$$

where  $\theta(n_1, n_2, n_r)$  is given by (4.2).

We wish to know, then, how many intertwiners exist with a given  $n_1, n_2$ , and  $n_r$ . This is found in the following lemma:

**Lemma 2** *If  $i$  is the number of edges (of colour 1) entering a branch, the number of distinct branches with internal edges  $\{a_2, a_3, \dots, a_i\}$  that end in a given edge label  $a_i$  is*

$$Q(i, a_i) = \frac{a_i + 1}{i + 1} \binom{i + 1}{\frac{a_i + i}{2} + 1} \quad (4.27)$$

**Proof:** Consider the network depicted in Figure 13. Given a sequence of internal edges  $\{a_1, a_2, \dots, a_n\}$ , we can define a path on this network which passes through the points  $\{(1, a_1), (2, a_2), \dots, (n, a_n)\}$ . Thus, the number of distinct branches with internal edges  $\{a_1, a_2, \dots, a_i\}$  is equal to the number of distinct paths on this lattice from the point  $x = 1, y = 1$  to the point  $x = i, y = a_i$  (which go strictly to the right at all times, not to the left.) We also note that  $Q(i, a_i) = Q(i - 1, a_i - 1) + Q(i - 1, a_i + 1)$ ; in other words, the number of paths to a given point in the network is equal to the sum of the numbers of paths to the two points closest to it in the previous column. Using this technique, the number of paths for small values of  $x$  and  $y$  can be easily calculated; these numbers are shown in Figure 13, above each vertex.

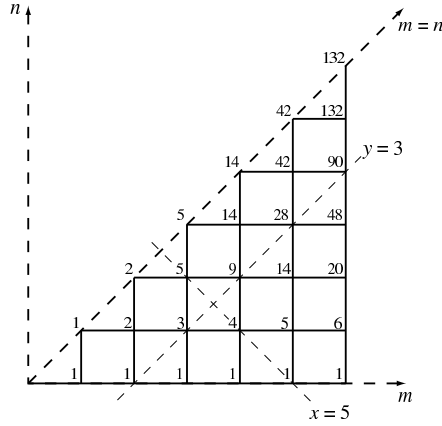


Figure 14: The lattice in the  $m$ - $n$  plane. To make the correspondence between this figure and Figure 13 clearer, we have included two representative lines of constant  $x$  and  $y$  in this diagram.

---

We now make the substitutions

$$m = \frac{x+y}{2} \quad \text{and} \quad n = \frac{x-y}{2};$$

note that  $m$  and  $n$  are integers since  $x \equiv y \pmod{2}$  for any point on our original lattice. If we redraw our lattice in the  $m$ - $n$  plane, we obtain Figure 14. Our paths are now on a conventional lattice; however, the condition that  $y \geq 0$  for the paths on our original lattice translates into the condition that  $m \geq n$  (since  $y = m - n$ .) Thus, we wish to find the number of lattice paths from  $(0, 0)$  to  $(m_0, n_0)$  (where  $m_0 = (i + a_i)/2$  and  $n_0 = (i - a_i)/2$ ) which never go above the line  $m = n$ .

This new problem is a classic problem in combinatorics; it is discussed, along with other related problems, by Hilton and Pedersen [21]. The result for the lattice paths is then

$$Q(m_0, n_0) = \frac{m_0 - n_0 + 1}{m_0 + n_0 + 1} \binom{m_0 + n_0 + 1}{m_0 + 1}$$

and the solution to our original problem is then

$$Q(i, a_i) = \frac{a_i + 1}{i + 1} \binom{i + 1}{\frac{i + a_i}{2} + 1}$$

If we wish to turn this into a normalized probability distribution, we can approximate the binomial coefficient in the above expression by a Gaussian distribution multiplied by a normalization factor  $A$ :

$$\binom{x}{y} = A \exp \left[ \frac{-(x - \frac{y}{2})^2}{\frac{y}{2}} \right]$$

Applying this to (4.27), we have

$$P(i, a_i) = \frac{a_i + 1}{i + 1} \exp \left[ \frac{-(a_i^2 + 2a_i)}{2(i + 1)} \right] \quad (4.28)$$

where  $A$  has been subsumed into the exponential term.

Using this probability distribution, we numerically computed the distribution of the angles in the interval  $[0, \pi]$ . The program randomly selected candidate values of  $n_1$ ,  $n_2$ , and  $n_r$ , making sure that they satisfied the vertex constraints; it then accepted or rejected the angle using the probability distribution derived above. The results for various values of  $s_1$ ,  $s_2$ , and  $s_r$  are shown in Figures 15 to 18.

Figure 15 shows the distribution for  $s_1 = s_2 = s_r$ . This distribution certainly does not match the expected classical distribution; most notable is the fact that the distribution peaks at approximately  $2.5 \approx 140^\circ$ .

Figures 16 and 17 show the distribution for  $s_1 = s_2 \ll s_r$  and  $s_1 < s_2 \ll s_r$ , respectively. These have surprisingly good correspondence with the expected classical angle distribution.

Figure 18 shows the case  $s_1 \ll s_2 \ll s_r$ . This particular case required an extraordinary amount of computer time; as a result, the deviation of the data points is much larger. However, the data still matches the expected  $\sin \theta$  distribution very well.

These data, while not conclusive, are certainly indicative that the angle operator can indeed reproduce the classical angle distribution in the case where  $s_1, s_2 \gg 1$  and  $s_1, s_2 \ll s_r$ . This first condition corresponds to what normally thinks of as a “classical limit,” well away from the regions where quantum effects dominate. The second condition can be thought of as a requirement for a sufficient amount of “background geometry”: not only do we need to make sure that the angles we are measuring include a large amount of spin, but we also need to ensure that the background spacetime upon which we measure the angles is sufficiently classical.

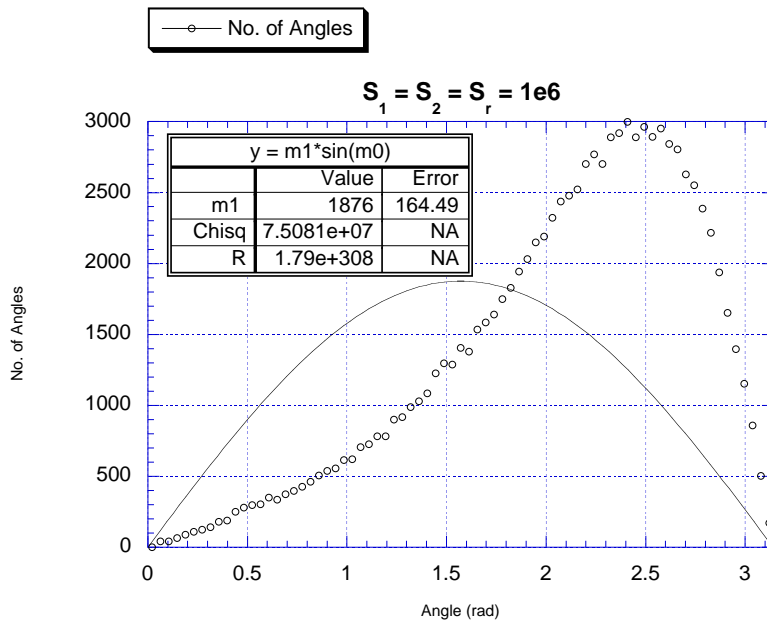


Figure 15: Angle distribution for  $s_1 = s_2 = s_r$ .

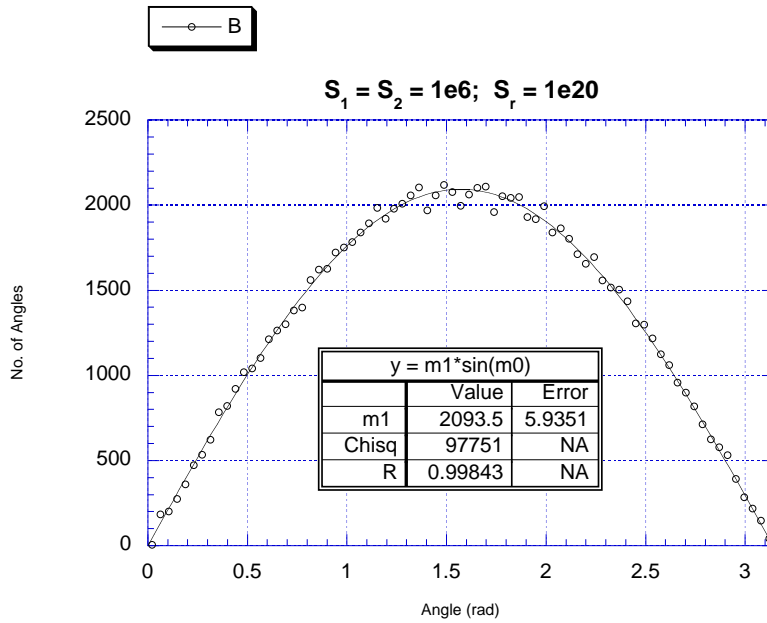


Figure 16: Angle distribution for  $s_1 = s_2 \ll s_r$ .

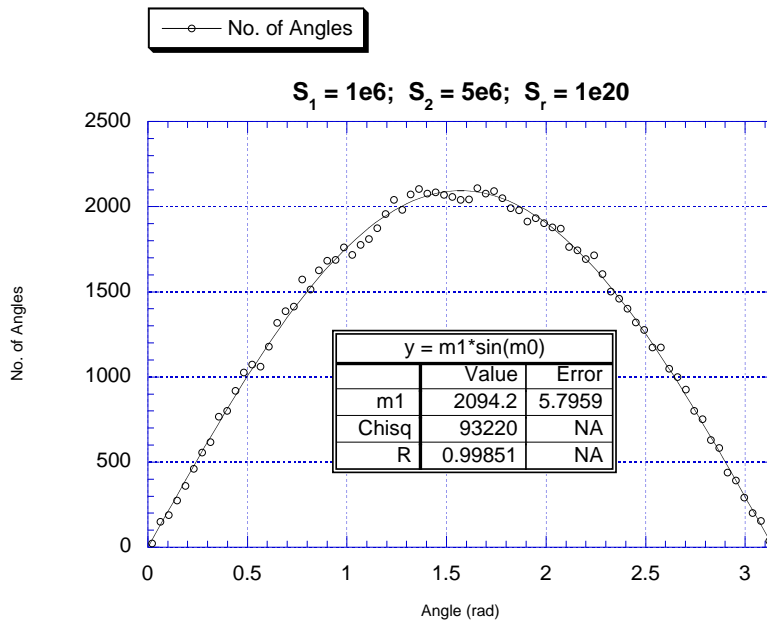


Figure 17: Angle distribution for  $s_1 < s_2 \ll s_r$ .

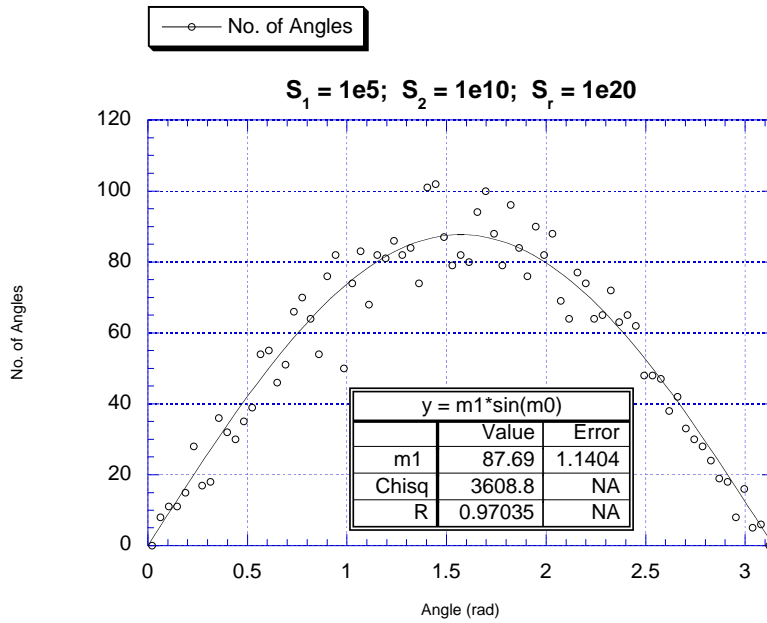


Figure 18: Angle distribution for  $s_1 \ll s_2 \ll s_r$ .

## 5 The Volume Operator

### 5.1 The $W$ -matrix and Eigenvalue Bounds

We recall from section 3.5.4 that the elements of the  $W$ -matrix are given by

$$W_{[rst]i_2 \dots i_{n-2}}^{(n) k_2 \dots k_{n-2}} = -P_r P_s P_t \begin{Bmatrix} k_2 & P_t & k_3 \\ i_2 & P_t & i_3 \\ 2 & 2 & 2 \end{Bmatrix} \lambda_{k_2}^{i_2} \delta_{i_4}^{k_4} \dots \delta_{i_{n-2}}^{k_{n-2}} \\ \times \frac{\begin{Bmatrix} P_r & P_r & P_0 \\ k_2 & i_2 & 2 \end{Bmatrix} \begin{Bmatrix} P_s & P_s & k_4 \\ k_3 & i_3 & 2 \end{Bmatrix}}{\theta(k_2, k_3, P_t)} \quad (5.1)$$

where  $k_2, \dots, k_{n-2}$  and  $i_2, \dots, i_{n-2}$  are the internal spins in the ‘‘comb’’ basis (see Figure 4.)

From this operator, we then define the ‘‘volume-squared’’ operator as

$$\hat{V}^2 = l_0^6 \sum_{r < s < t} \left| \frac{i \hat{W}_{[rst]}^{(n)}}{16} \right|, \quad (5.2)$$

where  $l_0$  is once again the Planck length. The eigenvalues of this operator are the squares of the volume operator  $\hat{V}$ .

We can see that this expression is horrendously difficult to handle in all its generality, for three main reasons. First, for an  $n$ -valent vertex with arbitrary edge colours, there are  $\binom{n}{3}$  possible choices for  $r$ ,  $s$ , and  $t$ ; each of these choices could conceivably produce a different  $W_{[rst]}^{(n)}$ . Second, the eigenvalues of the  $\hat{V}^2$  operator are difficult to find; even those of the  $W$ -matrix are distinctly non-trivial, since all that (5.1) gives us is the matrix entries. Third, the matrix entries themselves, as given by (5.1), are not easy to calculate analytically. These three factors make the overall problem rather intractable, either analytically or numerically.

With these problems, it is to our advantage to make some simplifications. Instead of considering an arbitrary vertex, we will examine the case of a monochromatic vertex; in this case, all of the matrices  $W_{[rst]}^{(n)}$  are identical (since our ‘‘graspings’’ are always on edges of the same colour.)<sup>20</sup> The formula (5.2) then reduces to

$$\hat{V}^2 = l_0^6 \binom{n}{3} \left| \frac{iW^{(n)}}{16} \right| = \frac{n(n-1)(n-2)}{96} |iW^{(n)}| \quad (5.3)$$

This solves our first problem. The second problem, however, is somewhat less tractable; analytically finding the eigenvalues of an  $n \times n$  matrix is equivalent to finding the roots of a  $n$ th degree polynomial, for which no analytic solution

<sup>20</sup>We will often suppress the indices  $[rst]$ , since they are always the same. In other words, when referring to the monochromatic case, we define  $W^{(n)} = W_{[rst]}^{(n)}$ .

exists for  $n > 4$ . The matrix  $W^{(n)}$ , on the other hand, has a row for each possible intertwiner core - a number that is, in general, much greater than 4. To get around this, we will examine bounds on the eigenvalues instead of the eigenvalues. For any  $n \times n$  matrix with entries  $a_{ij}$ , any given eigenvalue  $\lambda$  of this matrix satisfies

$$|\lambda| \leq \max_i \sum_{j=1}^n |a_{ij}| \quad \text{and} \quad |\lambda| \leq \max_j \sum_{i=1}^n |a_{ij}| \quad (5.4)$$

In other words, the magnitude of every eigenvalue must be less than the sum of the absolute values of some column and of some row.<sup>21</sup> Using this, we can find an upper bound  $M$  on the magnitudes of the eigenvalues of  $W^{(n)}$ . In the monochromatic case, however, the eigenvalues  $\lambda_{W\alpha}$  of the  $\hat{W}^{(n)}$  operator are related to the eigenvalues  $\lambda_{V^2\alpha}$  of the  $\hat{V}^2$  operator by

$$\lambda_{V^2\alpha} = \frac{n(n-1)(n-2)}{96} |\lambda_{W\alpha}| \quad (5.5)$$

as can be seen from (5.3). Hence, we can place a limit on the eigenvalues of the volume operator:

$$\begin{aligned} \lambda_{V\alpha} &= \sqrt{\lambda_{V^2\alpha}} \\ &= \sqrt{\frac{n(n-1)(n-2)}{96} |\lambda_{W\alpha}|} \\ &\leq \sqrt{\frac{n(n-1)(n-2)}{96}} M \end{aligned} \quad (5.6)$$

The determination of  $M$  — the last of our three problems above — is, unfortunately, rather intractable. While explicit expressions for the 6- $j$  and 9- $j$  symbols in (5.1) exist, they are rather complicated. Simpler expressions do exist for the case of a 4-valent vertex; in this case, we can easily calculate the matrix elements explicitly. However, in general, we will have great difficulty doing so.

---

<sup>21</sup> The other two well-known results for eigenvalue bounds — namely, Gershgorin's theorem and Schur's inequality — turn out to be much less useful to us. Gershgorin's theorem states that for some  $i$ ,

$$|\lambda - a_{ii}| \leq \sum_{j \neq i} |a_{ij}|$$

and a similar result for the rows of the matrix; however, the diagonal elements of the  $W^{(n)}$ -matrix are all zero, which reduces this formula to (5.4). Schur's inequality states that

$$\sum_{\alpha=1}^n |\lambda_{\alpha}|^2 \leq \sum_{i,j=1}^n |a_{ij}|^2$$

where  $\lambda_{\alpha}$  are the eigenvalues of the matrix. However, it is much more difficult to obtain an analytic expression for the RHS of this equation, as it includes all of the elements of the matrix. For more information on these bounds, consult Bell [22].

## 5.2 Volume Eigenvalue Bounds for 4-valent Vertices

In the case of a 4-valent vertex, De Pietri [17] has shown that the entries of the  $W^{(4)}$  matrix for a 4-valent vertex with edge colours  $a$ ,  $b$ ,  $c$ , and  $d$  are given explicitly by the formula

$$W_{[012]^{t-\epsilon}}^{(4) \ t+\epsilon} = \frac{-\epsilon(-1)^{(a+b+c+d)/2}}{32\sqrt{t(t+2)}} \frac{[(a+b+t+3)(c+d+t+3)(1+a+b-t)(1+c+d-t)(1+a+t-b)(1+b+t-a)(1+c+t-d)(1+d+t-c)]^{\frac{1}{2}}}{(5.7)}$$

where  $t + \epsilon$  and  $t - \epsilon$  correspond to the internal edge of the vertex. It can be shown that these elements are zero unless  $\epsilon = \pm 1$ ; hence, each row or column will have at most two non-zero elements. To find  $M$  in this case, then, all we have to do is to find the maximum value of the polynomial on the RHS of (5.7).

In the monochromatic case,  $a = b = c = d$ ; we will call this edge colour  $m$ . The polynomial in question then becomes

$$|W_{[012]^{t-\epsilon}}^{(4) \ t+\epsilon}| = \frac{(2m+t+3)(2m-t+1)(t+1)^2}{32\sqrt{t(t+2)}} \quad (5.8)$$

If we think of this as a continuous function  $W(t)$ , we can show that this expression is maximized at

$$t_{max} = \sqrt{\frac{(2m+2)^2+4}{6} + \frac{1}{6}\sqrt{(2m+2)^4-16(2m+2)^2+16}} - 1, \quad (5.9)$$

and the maximum value is, of course,  $W(t_{max})$ . In the large-spin limit, where  $m \gg 1$ , this maximum value scales as

$$|W_{max}| \approx \frac{m^3}{6\sqrt{3}} \quad (5.10)$$

The maximum absolute row or column sum (i.e. the quantity  $M$ ) is at most twice this number; therefore, (5.6) tells us that for a 4-valent monochromatic vertex with edge colour  $m \gg 1$ , any eigenvalue  $\lambda_V$  of the volume operator on this vertex will satisfy the inequality

$$\lambda_V \leq l_0^3 \frac{m^{3/2}}{\sqrt{12\sqrt{3}}} \quad (5.11)$$

This is a very encouraging result when we consider it in relation to the area operator. The eigenvalues of the area operator are given by

$$\lambda_A = l_0^2 \sum_i \sqrt{m_i(m_i+2)} \quad (5.12)$$



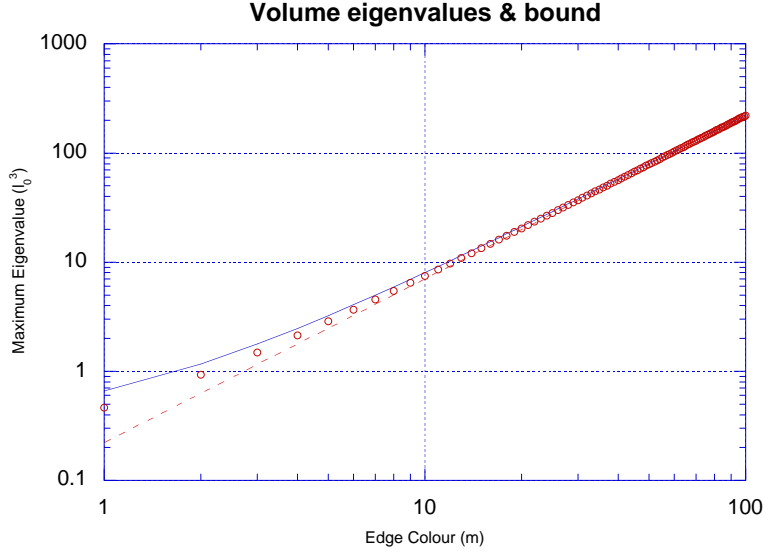


Figure 19: The eigenvalue limit (shown as a solid line) obtained in (5.8) and (5.9), compared with the maximum volume eigenvalue for  $1 \leq m \leq 100$  (shown as points). The lower dotted line is the result of a curve fit of the maximum eigenvalues to a curve of the form  $\lambda = km^{3/2}$ , where  $k$  is the only free parameter of the fit. This fit yields a value of  $k = 0.22155$ .

where the values  $m_i$  are all the intersections of edges with the surface in question. For a 4-valent vertex with large edge colour  $m$ , we have

$$\lambda_A \propto m. \quad (5.13)$$

Together with (5.11), this implies that the volume scales no faster than  $A^{3/2}$ , which is what we would expect from classical spatial geometry.

We must ask ourselves, however, how “good” this bound is: do the eigenvalues actually scale proportionally to  $m^{3/2}$ , and if so, is the proportionality coefficient we have found (i.e.  $1/\sqrt{12\sqrt{3}}$ ) close to the actual proportionality coefficient? Figure 19 shows the largest eigenvalue of the volume operator (found by numerical calculation) compared to the bound stated in (5.8) and (5.9). As we can see, the bound fits the volume eigenvalues very tightly, diverging significantly from them for  $n < 10$  and becoming practically indistinguishable from the maximum eigenvalue for  $n > 50$ . We also show, in Figure 20, the ratio between the eigenvalue bound we have found and the maximum eigenvalue. Note that this converges rapidly to 1.

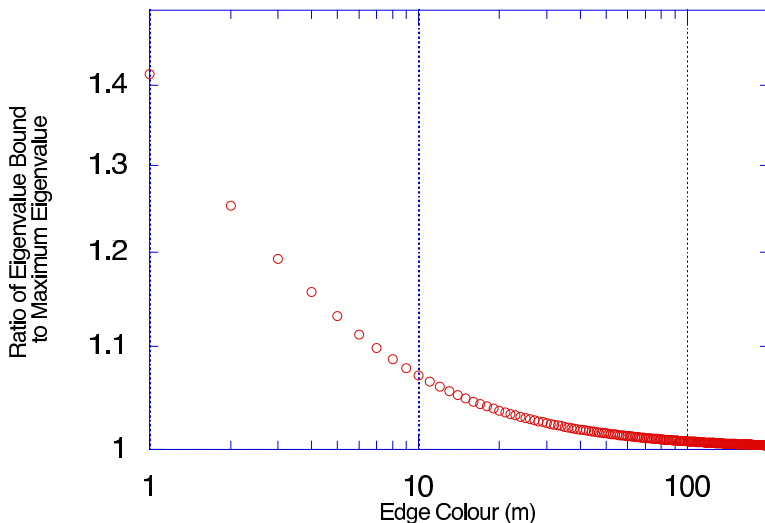


Figure 20: The ratio of the eigenvalue limit to the maximum volume eigenvalue, for  $1 \leq m \leq 200$ .

### 5.3 Eigenvalue Bounds for $n$ -Valent Vertices

We now turn our attention to the more general case of the  $n$ -valent monochromatic vertex. In this case, we cannot use the simple formula in (3.51), but must instead use the more general form in (3.42) or (3.43). There are some simplifications that can be made which aid us in computing these matrix entries and their bounds; however, a general analytic result is not forthcoming. Numerical methods, however, will prove fruitful.

First, we recall that we are examining the special case where  $P_r = P_s = P_t = P_0 = m$ . We note that the expression for the 9- $j$  symbol in (3.42) and (3.43) is fairly symmetric, and can be simplified. This symbol corresponds to the spin network

$$\left\{ \begin{array}{ccc} k_2 & m & k_3 \\ i_2 & m & i_3 \\ 2 & 2 & 2 \end{array} \right\} = \text{Diagram} \quad (5.14)$$

We can, however, move the grasplings of the 2-edges around using equation (B.10), and then close the resulting “triangles” using equation (B.11). Doing

this, we obtain

$$\left\{ \begin{array}{ccc} k_2 & m & k_3 \\ i_2 & m & i_3 \\ 2 & 2 & 2 \end{array} \right\} = \frac{\lambda_{k_3}^{i_3 2}}{m} \left( \frac{-i_2 \text{Tet} \begin{bmatrix} k_2 & i_2 & i_2 \\ 2 & 2 & 2 \end{bmatrix}}{\theta(k_2, i_2, 2)} + \frac{i_3 \text{Tet} \begin{bmatrix} k_3 & i_3 & i_3 \\ 2 & 2 & 2 \end{bmatrix}}{\theta(k_3, i_3, 2)} \right) \text{Tet} \begin{bmatrix} k_2 & k_3 & 2 \\ i_3 & i_2 & m \end{bmatrix}$$

Plugging this back in, (3.42) becomes

$$W_{[rst]i_2 \dots i_{n-2}}^{(n) k_2 \dots k_{n-2}} = -m^3 \mathcal{Q} \lambda_{k_2}^{i_2 2} \delta_{i_4}^{k_4} \dots \delta_{i_{n-2}}^{k_{n-2}} \times \frac{\text{Tet} \begin{bmatrix} m & m & m \\ k_2 & i_2 & 2 \end{bmatrix} \text{Tet} \begin{bmatrix} m & m & k_4 \\ k_3 & i_3 & 2 \end{bmatrix} \text{Tet} \begin{bmatrix} k_2 & k_3 & 2 \\ i_3 & i_2 & m \end{bmatrix} \Delta_{k_2} \Delta_{k_3}}{\theta(k_2, i_2, 2) \theta(k_3, i_3, 2) \theta(m, m, k_2) \theta(k_2, k_3, m) \theta(k_3, k_4, m)}$$

where

$$\mathcal{Q} = \frac{\lambda_{k_3}^{i_3 2}}{m} \left( \frac{-i_2 \text{Tet} \begin{bmatrix} k_2 & i_2 & i_2 \\ 2 & 2 & 2 \end{bmatrix}}{\theta(k_2, i_2, 2)} + \frac{i_3 \text{Tet} \begin{bmatrix} k_3 & i_3 & i_3 \\ 2 & 2 & 2 \end{bmatrix}}{\theta(k_3, i_3, 2)} \right) \quad (5.15)$$

We can also put the Tets in this resulting equation in terms of Wigner 6- $j$  symbols (see Appendix C); at least one of the arguments of the resulting Wigner 6- $j$  symbols will be 1, and analytic formulas for this case have been compiled (see, for example, Varshalovich [23]). Equation (3.42) then becomes

$$W_{[rst]i_2 \dots i_{n-2}}^{(n) k_2 \dots k_{n-2}} = -m^3 \mathcal{Q} \mathcal{R} \mathcal{S} \lambda_{k_2}^{i_2 2} \delta_{i_4}^{k_4} \dots \delta_{i_{n-2}}^{k_{n-2}} \quad (5.16)$$

where  $\mathcal{Q}$  is given in (5.15), and  $\mathcal{R}$  and  $\mathcal{S}$  are given by

$$\mathcal{R} = \left\{ \begin{array}{ccc} m/2 & k_2/2 & k_3/2 \\ 1 & i_3/2 & i_2/2 \end{array} \right\}_W \left\{ \begin{array}{ccc} m/2 & m/2 & k_2/2 \\ 1 & i_2/2 & m/2 \end{array} \right\}_W \left\{ \begin{array}{ccc} k_4/2 & m/2 & k_3/2 \\ 1 & i_3/2 & m/2 \end{array} \right\}_W \quad (5.17)$$

$$\mathcal{S} = \theta(m, m, 2) \sqrt{\frac{\theta(i_2, i_3, m) \theta(m, m, i_2) \theta(i_3, k_4, m)}{\theta(k_2, k_3, m) \theta(m, m, k_2) \theta(k_3, k_4, m)}} \quad (5.18)$$

Finally, we note that there are certain ‘‘selection rules’’ for finding the non-zero elements of  $W$  in this basis. The presence of a series of Kronecker deltas in (3.42) gives us the obvious selection rules that

$$k_4 = i_4, \quad k_5 = i_5, \quad \dots, \quad k_{n-2} = i_{n-2} \quad (5.19)$$

It is also evident from the spin diagram in (3.44) that for the 9- $j$  symbol in (3.42) to be non-zero, we must have

$$k_2 - i_2 = 0, \pm 2 \quad \text{and} \quad k_3 - i_3 = 0, \pm 2 \quad (5.20)$$

in order to satisfy the triangle inequalities. Finally, it can be shown that

$$\frac{a}{\theta(a, b, 2)} \text{Tet} \begin{bmatrix} a & a & b \\ 2 & 2 & 2 \end{bmatrix} = \begin{cases} (-1)^{a+1} \cdot \frac{a+2}{2} & b = a - 2 \\ -1 & b = a \\ (-1)^a \cdot \frac{a}{2} & b = a + 2 \\ 0 & \text{otherwise} \end{cases} \quad (5.21)$$

Hence, if  $k_2 = i_2$  and  $k_3 = i_3$ , the quantity in parentheses in (5.15) will be  $(-1 + 1)$ , with the result that  $\mathcal{Q} = 0$ . We can then rewrite (5.20) as

$$\begin{aligned} k_2 - i_2 = 0, \pm 2, \quad k_3 - i_3 = 0, \pm 2, \quad \text{and} \\ k_2 - i_2 \ \& \ k_3 - i_3 \ \text{are not both zero.} \end{aligned} \quad (5.22)$$

We conclude that for a given column of the  $W$  matrix (i.e. fixed  $k_2, k_3, \dots, k_{n-2}$ ), there will be at most eight non-zero elements:

$$\begin{aligned} i_2 = k_2 - 2 \quad i_2 = k_2 - 2 \quad i_2 = k_2 - 2 \\ i_3 = k_3 - 2 \quad i_3 = k_3 \quad i_3 = k_3 + 2 \\ \\ i_2 = k_2 \quad i_2 = k_2 \\ i_3 = k_3 - 2 \quad i_3 = k_3 + 2 \\ \\ i_2 = k_2 + 2 \quad i_2 = k_2 + 2 \quad i_2 = k_2 + 2 \\ i_3 = k_3 - 2 \quad i_3 = k_3 \quad i_3 = k_3 + 2 \end{aligned} \quad (5.23)$$

Unfortunately, this is about as far as analysis will easily take us. The quantities  $\mathcal{Q}$ ,  $\mathcal{R}$ , and  $\mathcal{S}$  are fairly simple to calculate for a given set of arguments; however, finding the maximum product of all three, over all possible values of  $\{k_2, k_3, k_4, i_2, i_3, i_4\}$  is a much more daunting task.<sup>22</sup> Things are complicated by the fact that both the quantities  $\mathcal{Q}$  and  $\mathcal{R}$  have slightly different analytic forms for each of the eight entries in a given column — one form for  $k_2 - i_2 = 2$  and  $k_3 - i_3 = 2$ , one form for  $k_2 - i_2 = 2$  and  $k_3 - i_3 = 0$ , and so forth (see Varshalovich [23].) We see, then, that an analytic answer is difficult to find.

Despite this difficulty, we can get an idea of the scaling properties of the absolute row and column sums by numerical analysis. By a happy coincidence, we do not even need to look at all of the rows and columns of the matrix — only a small subset of them. This is because (as mentioned above) the entries of the  $W$ -matrix are only dependent on the six values  $\{k_2, k_3, k_4, i_2, i_3, i_4\}$ ; all other pairs of corresponding indices must be equal, or the matrix entry will be

<sup>22</sup> Note that, in a small mercy granted to us by equation (5.1), the entries of this form of the  $W$ -matrix depend only on these six intertwiner strands (and the edge colour  $m$ ), and not on the entire set.

zero. These facts imply that the  $W$ -matrix must be of block-diagonal form, and that (more importantly) each one of the blocks is identical:

$$W = \begin{pmatrix} A & 0 & 0 & & 0 \\ 0 & A & 0 & \cdots & 0 \\ 0 & 0 & A & & 0 \\ & \vdots & & \ddots & \vdots \\ 0 & 0 & 0 & \cdots & A \end{pmatrix} \quad (5.24)$$

where each block corresponds to a different choice of  $k_5, \dots, k_{n-2}$ , and the indices of the matrix  $A$  are all possible choices for  $k_2, k_3$ , and  $k_4$ . We see that we need only compute the absolute row and column sums for the (much smaller) matrix  $A$ , instead of the full  $W$ -matrix. This is still a non-trivial calculation, as the size of the matrix  $A$  scales fairly quickly (for  $m = 10$ , the matrix has already grown to  $891 \times 891$ ), but it does simplify the problem greatly.

Using this trick, combined with the selection rules in (5.19) and (5.22), the bounding quantity  $M$  (as defined above in section 5.2) was calculated with MATLAB. Two methods were used. The first was the absolute row and column sum discussed previously. The second was MATLAB's internal `normest` function, which estimates the largest eigenvalue of a sparse matrix.<sup>23</sup> These results are shown in Figure 21. Each of these data sets is fitted to a power law relation. We see that for both of these data sets, we have an approximate relation  $M \propto m^3$ .

There is good reason to believe that this power dependence should tend towards  $m^3$  (exactly) as  $m \rightarrow \infty$ : if it does, then we have the relation

$$\begin{aligned} |\lambda_V| &\approx \sqrt{M \frac{n(n-1)(n-2)}{96}} \\ &\approx C\sqrt{m^3 n^3} \\ &= C(\text{total spin})^{3/2} \end{aligned} \quad (5.25)$$

where  $C$  is a proportionality constant. As noted in the previous section, this is the dependence expected from classical spatial geometry. While our data are not conclusive evidence of this relation, they are highly suggestive that this relation holds for a monochromatic vertex of any valence.

Thus, we have placed limits on the volume eigenvalues of monochromatic vertices; in both cases, we find that volume of a region scales as the  $3/2$  power of the area of its bounding surface. This result was found analytically in the 4-valent case; numerical results strongly suggest that this relation holds for the general case as well.

---

<sup>23</sup> For the mathematically inclined reader, we note that the absolute row and column sums are known as the 1-norm and the  $\infty$ -norm of a given matrix, respectively; that which `normest` finds is the 2-norm.

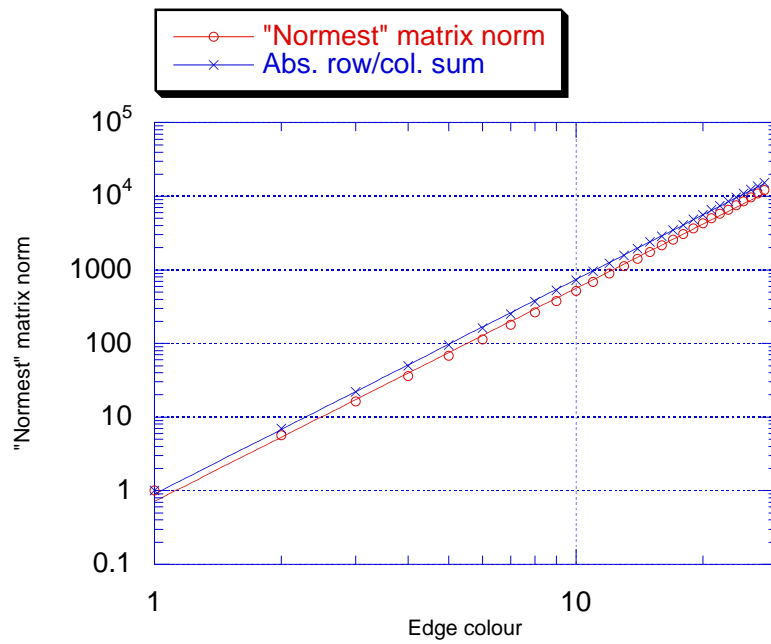


Figure 21: The eigenvalue limits found by the absolute row and column sums and by MATLAB's internal `normest` function. The curve fits are for a power law relation. For the absolute row/column sum method, the best fit is  $M = 0.90432 \cdot m^{2.9126}$ ; for the `normest` method, it is  $M = 0.71884 \cdot m^{2.8921}$ .

## 6 Discussion

We have seen some interesting consequences stemming from the discreteness of the angle operator (see Section 4); these results will be referred to as the *small angle* property (Equation 4.7), the *angular resolution* property (Equation 4.21), and the *angular distribution* property (Figures 15–18.) We now wish to assign some scaling behaviour to these predicted phenomena; in other words, on what length scales do we expect these phenomena to be observable?

The small angle property is the best-quantified of these three properties; we have the equation

$$\epsilon \geq \frac{4}{\sqrt{n_T + 8}} \geq \frac{4}{\sqrt{s_T + 8}}, \quad (6.1)$$

where  $s_T$  is the total surface flux. From our numerical studies of the volume operator, we also have the result that

$$V \propto \ell^3 \propto s_T^{3/2} \quad (6.2)$$

where  $\ell$  is the length scale (as defined by either the volume or area operator — we have shown that these are equivalent.) Hence, if we combine these results, we obtain the result that for large  $s_T$ , the minimum observable angle is related very simply to the length scale observed:

$$\epsilon \propto \ell^{-1} \propto s_T^{-1/2} \quad (6.3)$$

Moreover, from our discussion in Section 4.1, we recall that for a vertex with large amounts of “background geometry” (i.e.  $s_r \gg s_1, s_2$ ), the primary limit on  $n_T$  is not  $s_T$  but  $s_1 + s_2$ . Hence, for these vertices we have the result that

$$\epsilon \propto (s_1 + s_2)^{-1/2} \quad (6.4)$$

Using these relations, we can also gain an idea of the absolute length scale on which this phenomenon might be viewed. Recalling that

$$V = l_0^3 \sqrt{\frac{M}{96}} s_T^{3/2} \quad (6.5)$$

where  $M$  was found to be equal to 0.71884 (numerically), we can state an absolute relation between the length scale and the smallest observable angle:

$$\epsilon = k_\epsilon \left( \frac{\ell}{l_0} \right)^{-1} \quad (6.6)$$

where  $k_\epsilon = 4 \sqrt[6]{M/96} \approx 1.7692$ . This implies that if we observe angles on a length scale of  $\ell \approx 10^{-15}$  m (i.e. the radius of a proton), the minimum observable angle is then approximately  $10^{-20}$  radians — a miniscule angle by any account.

In Section 4.2, we found results for the mean angular resolution associated with a vertex. The most important of these was the average spacing between expectation values, given by

$$\delta \geq \frac{4\pi}{n^2 + 3n + 6}, \quad (6.7)$$

Again, combining these results with the result in (6.2) allows us to associate a scaling behaviour with the mean angular separation and resolution. For large  $n$ , the angular separation scales as

$$\delta \propto n^{-2} \propto \ell^{-4}, \quad (6.8)$$

This scaling property of the angular resolution is also somewhat striking, since it scales proportionally to such a high value of the total spin (i.e. inversely proportional to the fourth power of the length.)

Using similar techniques to those found above, we can find absolute length scales for  $\delta$  as well; these can be shown to be

$$\delta = k_\delta \left( \frac{\ell}{l_0} \right)^{-4} \quad (6.9)$$

where  $k_\delta = 4\pi(M/96)^{2/3} \approx 0.4810$ . On the length scale of a proton, this implies a resolution of roughly  $10^{-80}$  radians!

Finally, we found that we could reproduce a classical angle distribution under the condition that

$$1 \ll \{s_1, s_2\} \ll s_r. \quad (6.10)$$

This is somewhat harder to quantify; however, we *can* associate lengths with the distributions shown in Figures 15–18. For Figure 15, we have  $n_T \approx 10^6$ ; hence, the length scale associated with such a vertex is on the order of  $10^3 l_0 \approx 10^{-32}$  m; for Figures 16–18, the length scale would be on the order of  $10^{10} l_0 \approx 10^{-25}$  m. For reference, the diameter of an atomic nucleus is on the order of  $10^{-15}$  m, a full 17 orders of magnitude larger than the length scale associated with the “drastically altered” distribution of Figure 15. Even on a length scale ten orders of magnitude less than the size of a nucleus (as in Figures 16–18), the classical angle spectrum is reproduced.

We must be careful, however, that we do not read too much into these diagrams. The main difference between the conditions for the normal and skewed angle distributions is that  $s_1, s_2 \ll s_r$  for the former while  $s_1, s_2 \approx s_r$  for the latter. To gain a better understanding of where the transition between these two types of distribution actually occurs, we would have to examine the distributions over a wide range of values of  $s_1/s_r$  and  $s_2/s_r$ ; the results presented here only show two values of  $s_1/s_r$  and three of  $s_2/s_r$  (not counting the minor difference between Figures 16 and 17).

Moreover, while the skewed angle distribution in Figure 15 certainly occurs for  $s_1, s_2, s_r \approx 10^5$ , there is no reason to believe that this behaviour will go away



for larger values of the spins. If this behaviour does indeed persist at higher spins, our interpretation of the angle operator may be incorrect. We recall that the angle operator finds the angle between the two patches  $S_1$  and  $S_2$ ; perhaps all this distribution is telling us is that these patches don't "want" to overlap; as they get larger, they will have to spread themselves out to avoid each other. However, this is purely conjectural; more research is needed to find out whether this problem even arises.

The true importance of our angle distribution results becomes clearer when we consider them in light of the small-angle phenomenon. We recall that the smallest angle observable about a vertex depends on  $s_T$  if  $s_1, s_2 \approx s_r$ , but on  $s_1 + s_2$  if  $s_1, s_2 \ll s_r$ . To obtain a classical angle distribution, the latter of these conditions must hold; the magnitude of  $s_1$  and  $s_2$  then determines the minimum observable angle. Thus, if we have a vertex of a given spin, we have to balance two factors to obtain a classical angle distribution: the need to assign enough spin to  $s_r$  to obtain the correct distribution, along with the need to assign enough spin to  $s_1$  and  $s_2$ . Hence, to approximate classical angles in both of these ways, the total spin of the vertex must be sufficiently high.

## 7 Conclusion

The search for a quantum theory of gravity is one of the major challenges facing modern physics today. One of the more promising approaches in this search is the canonical or *loop quantum gravity* approach; in this theory, the fundamental variables of the theory are not field variables, but path integrals of field variables around closed loops in space. A difficulty arises from the properties of these loops: a given set of loops may satisfy any number of linear relations between themselves, making it difficult to compare two arbitrary states. This difficulty can be resolved through the use of *spin networks*, whose properties were described in Section 3.

Since general relativity predicts the structure of space, these spin networks must do so as well. This is done through Hermitian operators on spin network states, corresponding to “spatial observables” such as area, volume, and angle. While the forms of these last two operators are known, their properties have not been extensively studied.

Our research into the properties of these operators has revealed several peculiarities. In particular, we have shown that the minimum observable angle about a vertex with total spin  $s_T$  scales roughly as  $\epsilon \propto s_T^{-1/2}$ , a fairly slow decrease to zero. Moreover, since the angle operator has a discrete spectrum, the possible observable angles will be separated from each other. We have shown that the average separation between adjacent angles in the spectrum decreases as  $\delta \propto s_T^{-2}$ . Finally, we have shown that for “sufficiently classical” vertices (i.e.  $1 \ll \{s_1, s_2\} \ll s_r$ ), the classical angle distribution of  $\mathcal{P}(\theta) d\theta = \sin \theta d\theta$  is reproduced. However, in the case where  $s_1, s_2 \approx s_r$ , the angle distribution is vastly skewed from its normal behaviour.

Our studies of the volume operator were hindered by its complexity. However, we have found (through a combination of analytical and numerical methods) evidence suggesting that the volume associated with a vertex is proportional to the  $3/2$  power of a surface surrounding that vertex. This is identical to the scaling properties of these quantities in the classical model of space; hence, this result is a major step towards showing that spin networks can fully approximate classical continuum space.

The true measure of any theory, of course, is not how well it predicts already-observed effects but whether it predicts any new, hitherto unexpected phenomena. In this sense, our angle results are more important than our volume result. The latter result is still important, of course; if we had found any other dependence than  $(\text{volume}) \propto (\text{area})^{3/2}$ , we would have had to discard our current volume or area operator — if not the entire theory — as untenable. However, the fact that our angle results predict unexpected phenomena (the small-angle phenomenon and the skewed angle distribution) makes these results rather more interesting.

These phenomena imply that the angle operator predicts a drastically different structure of space for low-valence vertices. Unfortunately, such vertices are very far removed from our current realm of observation, even if we consider the next generations of observational equipment. To get a rough idea of how

far away we are from experimentally probing the predicted properties of spin networks, we can note that to do so would require a particle with a de Broglie wavelength on the order of the Planck length. Hence, such a particle would have a momentum

$$p_0 = \frac{h}{l_0} \approx 3 \times 10^{28} \text{ eV}/c \approx 16 \text{ kg} \cdot \text{m/s}. \quad (7.1)$$

While this may not seem like terribly much momentum on a macroscopic scale, it is a tremendous amount of energy for an elementary particle to have. If we make the assumption that the rest mass of such a particle is very small (i.e.  $m_0 \ll p_0/c \approx 50 \mu\text{g}$ ), its energy will be (to first order) determined by its momentum only:

$$E = p_0 c \approx 3 \times 10^{28} \text{ eV} \approx 5 \text{ GJ}. \quad (7.2)$$

This is a stupendous amount of energy; for comparison, the kinetic energy of a cruising Boeing 747 is roughly 12 gigajoules. We cannot possibly hope, then, to probe these distances directly at any point in the near future.

Because of this, the skewed angle distribution result is rather interesting: it predicts a change in angle distributions at a scale three orders of magnitude larger than the Planck length. This would bring down the required energy of a particle required to see this phenomenon to approximately  $10^{-25} \text{ eV}$  — still well beyond our observational capability, but a good deal closer. However, as mentioned in Section 6, this result is still open to interpretation. The normal distributions shown in Figures 16–18, however, do place an upper bound on the length scales on which quantum angle effects can be observed — by the time we have reached a length scale of  $10^{-25} \text{ m}$ , the quantum angle spectrum approximates the classical angle spectrum very well.

In the face of this, the small-angle property may end up being the “best” prediction stemming from our results. This is not to denigrate the other results we have found; the angle distribution and volume results show that the angle and volume operators do satisfy “classical” relations on a large scale. These are important properties for an quantum theory of general relativity to have, and are important steps towards showing that loop quantum gravity is a self-consistent example of such a theory.

## Appendices

### A Dirac-Bergmann Constraint Analysis

#### A.1 The Generalized Hamiltonian

To canonically quantize a classical theory, we need first to find a general expression for its Hamiltonian. It is fairly simple to find one Hamiltonian for a given system; however, our objective is to find an expression for all the possible Hamiltonian of a given theory. Such an expression should permit arbitrary variations that are implicit in the theory (e.g. gauge freedom in classical electrodynamics.) The following derivation of the generalized Hamiltonian follows from Dirac [25].

To construct the generalized Hamiltonian, it is easiest to start from the point of the action integral:

$$S = \int L(q_1, q_2, \dots, q_N, \dot{q}_1, \dot{q}_2, \dots, \dot{q}_N) dt \quad (\text{A.1})$$

where  $\{q_1, q_2, \dots, q_N\}$  are the coordinates of the configuration space of the system, and  $\{\dot{q}_1, \dot{q}_2, \dots, \dot{q}_N\}$  are their time derivatives. By applying the calculus of variations to this integral, we obtain the Lagrangian equations of motion:

$$\frac{\partial L}{\partial q_n} - \frac{d}{dt} \left( \frac{\partial L}{\partial \dot{q}_n} \right) = 0 \quad (\text{A.2})$$

Note that there are  $N$  such equations, one for each coordinate of the configuration space.

The Hamiltonian formalism first requires us to change variables from the velocities  $\dot{q}_n$  to the conjugate momenta  $p_n$ :

$$p_n = \frac{\partial L}{\partial \dot{q}_n} \quad (\text{A.3})$$

These momenta will satisfy the Poisson bracket relation

$$\{q_n, p_m\} = \delta_{nm}, \quad (\text{A.4})$$

where the *Poisson bracket* of two quantities  $f$  and  $g$  is defined as

$$\{f, g\} = \frac{\partial f}{\partial q_n} \frac{\partial g}{\partial p_n} - \frac{\partial f}{\partial p_n} \frac{\partial g}{\partial q_n}. \quad (\text{A.5})$$

It is possible that these momenta are all independent of one another; however, this is not required in general. As a simple example, consider a disc rolling without slipping on a plane. The disc's linear momentum  $p_x$  is not independent of its angular momentum  $p_\theta$ .

There will therefore be a certain number of constraints on the coordinates and momenta. These constraints can be written in the form

$$\phi_m(q, p) = 0 \quad m = 1, 2, \dots, \mathcal{M} \quad (\text{A.6})$$

where  $q$  and  $p$  denote any combination of the coordinates and the conjugate momenta. The expressions in (A.6) are called the *primary constraints* of the formalism.

Let us now consider the quantity  $H = p_n \dot{q}_n - L$ . We first note that an arbitrary variation in this quantity can be expressed as

$$\begin{aligned}\delta H &= \delta p_n \dot{q}_n + p_n \delta \dot{q}_n - \frac{\partial L}{\partial q_n} \delta q_n - \frac{\partial L}{\partial \dot{q}_n} \delta \dot{q}_n \\ &= \delta p_n \dot{q}_n - \frac{\partial L}{\partial q_n} \delta q_n,\end{aligned}\tag{A.7}$$

Thus, a variation in  $H$  can be expressed solely in terms of variations in  $p_n$  and  $q_n$ ; this implies that  $H$  is solely a function of the coordinates and their conjugate momenta, and not of their velocities  $\dot{q}_n$ .

This quantity  $H$  is called the *Hamiltonian* of the system. However, it is not uniquely determined. Since the primary constraints are identically zero, we can add any combination of them to the Hamiltonian without changing the Hamiltonian's value:

$$H^* = H - u_m \phi_m\tag{A.8}$$

where the coefficients  $u_m$  are arbitrary. (The negative sign is chosen merely for notational convenience later.) Using this new Hamiltonian, we can then deduce the generalized Hamiltonian equations of motion from (A.7) and (A.8):

$$\begin{aligned}\frac{\partial H^*}{\partial p_n} &= \dot{q}_n - u_m \frac{\partial \phi_m}{\partial p_n} - \frac{\partial u_m}{\partial p_n} \phi_m \\ \frac{\partial H^*}{\partial q_n} &= -\frac{\partial L}{\partial q_n} - u_m \frac{\partial \phi_m}{\partial q_n} - \frac{\partial u_m}{\partial q_n} \phi_m\end{aligned}$$

Noting that the primary constraints vanish and applying (A.2) to the second equation, these equations lead to the *Hamiltonian equations of motion*:

$$\dot{q}_n = \frac{\partial H}{\partial p_n} + u_m \frac{\partial \phi_m}{\partial p_n}\tag{A.9}$$

$$\dot{p}_n = -\frac{\partial H}{\partial q_n} - u_m \frac{\partial \phi_m}{\partial q_n}\tag{A.10}$$

We can rewrite these equations in a fairly simple form using Poisson bracket notation. The time evolution of any quantity  $g(q, p)$  is given by

$$\dot{g} = \frac{\partial g}{\partial q_n} \dot{q}_n + \frac{\partial g}{\partial p_n} \dot{p}_n\tag{A.11}$$

Applying (A.9) and (A.10), we see that

$$\begin{aligned}
\dot{g} &= -\frac{\partial g}{\partial p_n} \left( \frac{\partial H}{\partial q_n} + u_m \frac{\partial \phi_m}{\partial q_n} \right) + \frac{\partial g}{\partial q_n} \left( \frac{\partial H}{\partial p_n} + u_m \frac{\partial \phi_m}{\partial p_n} \right) \\
&= \left( \frac{\partial g}{\partial q_n} \frac{\partial H}{\partial p_n} - \frac{\partial g}{\partial p_n} \frac{\partial H}{\partial q_n} \right) + \left[ \frac{\partial g}{\partial q_n} \left( u_m \frac{\partial \phi_m}{\partial p_n} + \phi_m \frac{\partial u_m}{\partial p_n} \right) \right. \\
&\quad \left. + \frac{\partial g}{\partial p_n} \left( u_m \frac{\partial \phi_m}{\partial q_n} + \phi_m \frac{\partial u_m}{\partial q_n} \right) \right] \\
&= \frac{\partial g}{\partial q_n} \frac{\partial (H + u_m \phi_m)}{\partial p_n} - \frac{\partial g}{\partial p_n} \frac{\partial (H + u_m \phi_m)}{\partial q_n} \\
&= \{g, H_T\}
\end{aligned} \tag{A.12}$$

where  $H_T = H + u_m \phi_m$  is the *total Hamiltonian*. Note that the extra terms introduced in the second step are identically zero.

This formulation of the Hamiltonian equations of motion is concise; however, it does pose a potential pitfall. Our primary constraints  $\phi_m$  are, by definition, equal to zero; however, if we were to apply this equality immediately, before working out the Poisson brackets in (A.12), we would lose the generality that they allow. To clarify this distinction, we introduce the concept of “weak equality”, denoted

$$\phi_m \approx 0 \tag{A.13}$$

This notation signifies that one may only make use of this relation after the Poisson brackets have been worked out. Using this notation, then, (A.12) becomes

$$\dot{g} \approx \{g, H_T\}. \tag{A.14}$$

We can use (A.14) to check for further consistency conditions of the theory. If we apply (A.14) to one of the primary constraints  $\phi_m$ , we have

$$\dot{\phi}_m \approx 0 \approx \{\phi_m, H\} + u_{m'} \{\phi_m, \phi_{m'}\} \tag{A.15}$$

Thus, for each value of  $m$ , we have a consistency condition. Each one of these conditions leads to one of three results:<sup>24</sup>

- The equations in (A.15) could lead to an equation that is trivially satisfied, i.e. of the form  $0 = 0$ .
- The consistency conditions could reduce to an equation that contains only coordinates and momenta. Such a condition must be independent of the primary constraints (otherwise, it would be identically zero and therefore be of the first type.) We therefore have a new set of *secondary constraints*:

$$\phi_k(q, p) \approx 0 \quad k = \mathcal{M} + 1, \mathcal{M} + 2, \dots, \mathcal{K} \tag{A.16}$$

---

<sup>24</sup>It is possible that one or more of these equations lead directly to an inconsistency (i.e. an equation of the form  $1 = 0$ ); in this case, our original Lagrangian equations of motion were inconsistent, and the theory must be modified or rejected.

- Finally, the consistency conditions may not reduce in either of the above ways; in this case, they impose a constraint on the unknown functions  $u_m$ .

Secondary constraints may themselves generate other constraints by further applications of (A.14), i.e.

$$\{\phi_k, H\} + u_m \{\phi_k, \phi_m\} \approx 0, \quad (\text{A.17})$$

where  $k > \mathcal{M}$ . These new constraints may be of any one of the three types listed above. If they turn out to be new secondary constraints, we can continue to apply (A.14) recursively to them. In the end, we are left with our original set of primary constraints  $\phi_m$ , a new set of secondary constraints  $\phi_k$ , and a set of equations of the third type relating the  $u_m$ 's.

Let us further examine these equations of the third type. Each of these equations is of the form

$$\{\phi_j, H\} + u_m \{\phi_j, \phi_m\} \approx 0 \quad j = 1, 2, \dots, \mathcal{K} \quad (\text{A.18})$$

We can consider (A.18) to be a system of  $\mathcal{K}$  linear non-homogeneous equations, with the  $u_m$ 's as variables and coefficients in terms of the commutators of the primary and secondary constraints. Since these coefficients are in terms of  $p$ 's and  $q$ 's, we conclude that the  $u_m$ 's must also be functions of the coordinates and the momenta:

$$u_m = U_m(p, q) \quad (\text{A.19})$$

A complete solution for these variables also includes an arbitrary linear combination of the independent solutions (if any) to the homogeneous system of equations

$$V_m \{\phi_j, \phi_m\} = 0. \quad (\text{A.20})$$

Hence, the general solution to this system of equations is

$$u_m = U_m + v_a V_{am}, \quad (\text{A.21})$$

where  $a$  sums over the solutions found in (A.20). The total Hamiltonian can then be written as

$$H_T = H' + v_a \phi_a \quad (\text{A.22})$$

where

$$H' = H + U_m \phi_m \quad (\text{A.23})$$

and

$$\phi_a = V_{am} \phi_m. \quad (\text{A.24})$$

It is important to note that while the original  $u_m$  coefficients were not necessarily independent of one another, the new coefficients  $v_m$  in (A.22) are totally independent.<sup>25</sup>

At this point, we introduce a bit of nomenclature. We call a dynamical variable  $R$  *first-class* if its Poisson brackets with every constraint (primary and secondary) are weakly zero:

$$\{R, \phi_j\} \approx 0 \quad (\text{A.25})$$

An expression that is weakly zero must be equal to some linear combination of the constraints; hence, we have

$$\{R, \phi_j\} = c_{jj'} \phi_{j'} \quad (\text{A.26})$$

If  $R$  does not satisfy (A.25) for each  $\phi_j$ , we say that  $R$  is *second-class*. The “class” of a constraint is independent of whether it is a primary or secondary constraint; hence, we now have a total of four types of constraints.

Let us again consider the arbitrary coefficients  $v_a$  in (A.22). These new coefficients enter into the equations of motion:

$$\dot{g} \approx \{g, H' + v_a \phi_a\} \quad (\text{A.27})$$

However, a classical theory such as ours should be deterministic; we must therefore inquire as to the meaning of these arbitrary coefficients in the equations of motion.

Initially, the state of the system is determined solely by the coordinates and momenta, not by the  $v_a$ 's. If the theory is deterministic, then this state uniquely determines the system's later state. However, since the evolution of the coordinates and momenta depends on the values of the coefficients  $v_a$ , certain values of coordinates and momenta must correspond to the same physical state. To determine the relations between these values, we consider an infinitesimal time evolution in any dynamical variable  $g$ :

$$\begin{aligned} \delta_t g &= g_0 + \dot{g} \delta t \\ &= g_0 + \{g, H_T\} \delta t \\ &= g_0 + \delta t (\{g, H'\} + v_a \{g, \phi_a\}) \end{aligned} \quad (\text{A.28})$$

The  $v_a$  coefficients are completely arbitrary; thus, we change them to obtain a new  $\delta_t g$ . Since our theory is deterministic, these two new  $g$ 's must correspond to the same state; therefore, the difference between them must correspond to a transformation that does not change the state:

$$\begin{aligned} \Delta g &= \delta t (v_a - v'_a) \{g, \phi_a\} \\ &\equiv \epsilon_a \{g, \phi_a\} \end{aligned} \quad (\text{A.29})$$

---

<sup>25</sup>In general, there will be fewer of the  $v_m$ 's than of the  $u_m$ 's.



We can therefore change  $g$  using this rule, and the physical state will remain the same. These are known as *infinitesimal canonical transformations*, and the  $\phi_a$ 's are their generators.<sup>26</sup>

Suppose we apply two such transformations successively. We obtain

$$\begin{aligned} g &\mapsto g + \epsilon_a \{g, \phi_a\} \\ &\mapsto g + \epsilon_a \{g, \phi_a\} + \gamma_{a'} \{g + \epsilon_a \{g, \phi_a\}, \phi_{a'}\} \equiv g' \end{aligned} \quad (\text{A.31})$$

If we apply them in the opposite order instead, we get

$$g \mapsto g + \gamma_{a'} \{g, \phi_{a'}\} + \epsilon_a \{g + \gamma_{a'} \{g, \phi_{a'}\}, \phi_a\} \equiv g'' \quad (\text{A.32})$$

Since these two values of  $g$  correspond to the same physical state, a transformation corresponding to their difference must also be an infinitesimal canonical transformation that is not associated with a change of state:

$$\begin{aligned} g' - g'' &= \epsilon_a \{g, \phi_a\} + \gamma_{a'} \{g, \phi_{a'}\} + \gamma_{a'} \epsilon_a \{ \{g, \phi_a\}, \phi_{a'} \} \\ &\quad - \gamma_{a'} \{g, \phi_{a'}\} - \epsilon_a \{g, \phi_a\} - \epsilon_a \gamma_{a'} \{ \{g, \phi_{a'}\}, \phi_a \} \\ &= \epsilon_a \gamma_{a'} ( \{ \{g, \phi_a\}, \phi_{a'} \} + \{ \{ \phi_{a'}, g \}, \phi_a \} ) \\ &= \epsilon_a \gamma_{a'} ( \{g, \{ \phi_a, \phi_{a'} \} \} ) \end{aligned} \quad (\text{A.33})$$

We see that the commutators of the  $\phi_a$ 's can also generate infinitesimal canonical transformations. However, it is important to note that while the original set of canonical transformations were generated by primary constraints, the new transformations generated by the commutators are not necessarily primary constraints.

This leads us to the *extended Hamiltonian*  $H_E$ , which consists of the total Hamiltonian  $H_T$  plus any linear combination of expressions  $\phi_{a'}$  which generate infinitesimal canonical transformations not associated with a change of state:

$$H_E = H_T + v'_{a'} \phi_{a'} \quad (\text{A.34})$$

We will find in the next section that in the case of electrodynamics, these canonical transformations will correspond to gauge transformations. This last equation, then, is the most general expression for the Hamiltonian of a system.

## A.2 Dirac-Bergmann Analysis & Electrodynamics

As an example of Dirac-Bergmann analysis, let us attempt to construct the generalized Hamiltonian for classical electrodynamics. We saw in Section 2.1 that the *field tensor* is given by

$$F_{\mu\nu} = \partial_\mu A_\nu - \partial_\nu A_\mu. \quad (\text{A.35})$$

---

<sup>26</sup>For our purposes, we will consider an infinitesimal canonical transformation to be a transformation that adds an arbitrary infinitesimal (possibly a function of the original variable) to  $g$ , e.g.

$$g \mapsto g + \epsilon_a \{g, \phi_a\} \quad (\text{A.30})$$

In the above equation,  $\phi_a$  is called the *generator* of the infinitesimal contact transformation. For further explanation of canonical transformations, consult Goldstein [26].

In terms of this tensor, the action can be shown to be

$$S[A_\mu] = -\frac{1}{4} \int F^{\mu\nu} F_{\mu\nu} d^4\mathbf{x} \quad (\text{A.36})$$

where the integral is taken over a region of spacetime.

Constructing the momenta from the action requires a Lagrangian; normally this Lagrangian is related to the action by the relation  $S = \int L dt$ . To obtain our Lagrangian, then, we must define a reference frame; this defines a  $t$ -direction on spacetime. We can then split the four-dimensional integral in (A.36) into a double integral over space and time:

$$S = -\frac{1}{4} \iint F^{\mu\nu} F_{\mu\nu} d^3\mathbf{x} dt \quad (\text{A.37})$$

The Lagrangian is then the spatial part of this equation:

$$L = -\frac{1}{4} \int F^{\mu\nu} F_{\mu\nu} d^3\mathbf{x} \quad (\text{A.38})$$

In a simple particle-dynamics system, we find the momenta by taking the derivative of the Lagrangian with respect to velocities, as in (A.3). Taking the derivative with respect to a field, however, is less straightforward.

To find these momenta, we first define the *Lagrangian density* as a scalar field over all space:

$$\mathcal{L}(\mathbf{x}) = -\frac{1}{4} F^{\mu\nu}(\mathbf{x}) F_{\mu\nu}(\mathbf{x}) \quad (\text{A.39})$$

Note that this is simply the integrand of (A.38). The momenta, which we rather suggestively label  $E^\mu$ , are then defined by

$$E^\mu(\mathbf{x}) = \frac{\partial \mathcal{L}(\mathbf{x})}{\partial \dot{A}_\mu(\mathbf{x})} \quad (\text{A.40})$$

To find these explicitly, we split the Lagrangian density into time-dependent and non-time-dependent parts:

$$\mathcal{L} = -\frac{1}{4} (F^{00} F_{00} + F^{a0} F_{a0} + F^{0a} F_{0a} + F^{ab} F_{ab}) \quad (\text{A.41})$$

The first term of this expression vanishes, since  $F_{\mu\nu}$  is anti-symmetric. Moreover, the last term does not contain any terms containing the velocities (i.e. terms of the form  $\partial_0 A_\mu$ ), so we can discard it when taking the derivatives:

$$\begin{aligned} E^\mu &= \frac{\partial \mathcal{L}}{\partial \dot{A}_\mu} \\ &= -\frac{1}{4} \frac{\partial}{\partial \dot{A}_\mu} (F^{a0} F_{a0} + F^{0a} F_{0a}) \\ &= -\frac{1}{2} \frac{\partial}{\partial \dot{A}_\mu} (F^{a0} (\partial_a A_0 - \partial_0 A_a) + F^{0a} (\partial_0 A_a - \partial_a A_0)) \end{aligned}$$

Recalling that  $\dot{A}_\mu = \partial_0 A_\mu$  and that  $F^{0a} = -F^{a0}$ , this reduces to

$$E^\mu = F^{\mu 0}. \quad (\text{A.42})$$

We see now why the symbol  $E^\mu$  was used to denote the momenta: the momenta turn out to be the components of the electric field. Moreover, since  $E^0 = F^{00} = 0$ , we can discard the  $t$ -component of this vector; hence, we will also denote the electric field as  $E^a$ . Moreover, since  $E^0 = 0$ , its conjugate variable  $A_0$  is not physically significant (i.e.  $A_0$  is a cyclic variable); hence, we will denote the configuration variable as  $A_a$  as well. However, it is important to note that these constraints are only weakly equal to 0; to retain all generality, we will have to retain  $E^0$  and  $A_0$  until we have found the secondary constraints.

The Poisson brackets of the configuration variables  $A_a$  and  $E^a$  will then satisfy the relations

$$\begin{aligned} \{E^a(x), E^b(y)\} &= 0 \\ \{A_a(x), A_b(y)\} &= 0 \\ \{A_a(x), E^b(y)\} &= \delta_a^b \delta^3(x-y) \end{aligned} \quad (\text{A.43})$$

Now that we have the momenta, we can construct the Hamiltonian for the electromagnetic field:

$$\begin{aligned} H &= \int E^\mu \partial_0 A_\mu \, d^3\mathbf{x} - L \\ &= \int F^{a0} \partial_0 A_a + \frac{1}{4} (F^{00} F_{00} + F^{a0} F_{a0} + F^{0a} F_{0a} + F^{ab} F_{ab}) \, d^3\mathbf{x} \\ &= \int F^{a0} (\partial_a A_0 - F_{a0}) + \frac{1}{2} F^{a0} F_{a0} + \frac{1}{4} F^{ab} F_{ab} \, d^3\mathbf{x} \end{aligned}$$

where we have used the relation  $\partial_0 A_a = \partial_a A_0 - F_{a0}$  in the first term and collected two terms together to make the second (through the symmetry of  $F$ .) Rearranging and combining terms, we have

$$\begin{aligned} H &= \int \frac{1}{4} F^{ab} F_{ab} - \frac{1}{2} F^{a0} F_{a0} + F^{a0} \partial_a A_0 \, d^3\mathbf{x} \\ &= \int \frac{1}{4} F^{ab} F_{ab} + \frac{1}{2} E^a E_a - A_0 \partial_a E^a \, d^3\mathbf{x} + \int A_0 E^a n_a \, d^2\mathbf{x} \end{aligned} \quad (\text{A.44})$$

Note that we have applied an integration by parts in this last step, creating the last term of the three-dimensional integral and the surface integral; the sign of the second term also changes since  $F^{a0} = -E^a$ . This shows that the Hamiltonian is not dependent on the velocities  $\dot{A}_\mu$ , as desired. The final term, in which  $n_a$  is a vector normal to the surface enclosing the region being integrated, can be ignored if we assume that the strength of the electric field falls off at least as fast as  $1/r^2$ .

Our next step is to examine the constraints. We have already found one constraint from the antisymmetry of the field tensor, namely that

$$E^0(\mathbf{x}) \approx 0. \quad (\text{A.45})$$

We note that this is a constraint on  $E^0(\mathbf{x})$  at every point in the three-space under consideration. To find the secondary constraint associated with this primary constraint, we examine the time evolution of  $E^0(\mathbf{x})$ :

$$\begin{aligned} \dot{E}^0(\mathbf{x}) &\approx 0 \\ [E^0, H] &\approx 0 \\ \frac{\partial E^0(\mathbf{x})}{\partial A_0(\mathbf{x})} \frac{\partial H}{\partial E^0(\mathbf{x})} - \frac{\partial E^0(\mathbf{x})}{\partial E^0(\mathbf{x})} \frac{\partial H}{\partial A_0(\mathbf{x})} &= 0 \\ \frac{\partial}{\partial A_0(\mathbf{x})} \left( \int A_0(\mathbf{x}) \partial_a E^a(\mathbf{x}) d^3\mathbf{x} \right) &= 0 \\ \int \left( \frac{\partial A_0(\mathbf{x})}{\partial A_0(\mathbf{x})} \partial_a E^a(\mathbf{x}) + A_0(\mathbf{x}) \frac{\partial}{\partial A_0(\mathbf{x})} (\partial_a E^a(\mathbf{x})) \right) d^3\mathbf{x} &= 0 \end{aligned}$$

The second term is zero, since the momenta are totally independent of the coordinates. Since the integral of the first term must be zero for a variation of the field at any point in space  $\mathbf{x}$ , it follows that the secondary constraint associated with (A.45) is

$$\partial_a E^a(\mathbf{x}) \approx 0. \quad (\text{A.46})$$

The reader may note that this is Gauss' law in the absence of charge; this makes sense, since we have been examining the source-free versions of the Maxwell equations. If we examine the time evolution of this new constraint, we find that the equation reduces identically to zero; hence, we have one primary constraint and one secondary constraint for this Hamiltonian. It can be shown that these constraints are both first-class.

The total Hamiltonian of the electromagnetic field is then given by

$$H_T = \int \frac{1}{4} F^{ab} F_{ab} + \frac{1}{2} E^a E_a d^3\mathbf{x} - \int A_0 \partial_a E^a d^3\mathbf{x} + \int v(\mathbf{x}) E^0 d^3\mathbf{x}, \quad (\text{A.47})$$

where  $v(\mathbf{x})$  is an arbitrary scalar function over all of the region of integration. To obtain the extended Hamiltonian, we add in the secondary constraints:

$$H_E = H_T + \int u(\mathbf{x}) \partial_a E_a d^3\mathbf{x} \quad (\text{A.48})$$

where  $u(\mathbf{x})$  is another arbitrary scalar function. We note the similarity of this term to the third term of the total Hamiltonian; this suggests that  $A_0$  does not have any physical significance, since it can have an arbitrary coefficient added to it. If we wish to discard all variables without physical significance, we can also drop the final term of the total Hamiltonian (involving the term  $E^0 = 0$ ), to obtain a new Hamiltonian

$$H = \int \frac{1}{4} F^{ab} F_{ab} + \frac{1}{2} E^a E_a + u(\mathbf{x}) \partial_a E_a d^3\mathbf{x}. \quad (\text{A.49})$$

This Hamiltonian has the advantage of containing no reference to the unphysical variables  $A_0$  and  $E^0$ , while still retaining some gauge freedom (in terms of the function  $u(\mathbf{x})$ .)

Finally, we note that this expression is not as unfamiliar as it might seem. The first term of (A.49) can be written as

$$\frac{1}{4}F^{ab}F_{ab} = \frac{1}{2}(B_x^2 + B_y^2 + B_z^2) \quad (\text{A.50})$$

(where the extra factor of two comes from the fact that we have summed both the term  $F^{ab}F_{ab}$  and  $F^{ba}F_{ba}$ .) Similarly, the second term can be written as

$$\frac{1}{2}E^a E_a = \frac{1}{2}(E_x^2 + E_y^2 + E_z^2) \quad (\text{A.51})$$

Noting that  $\partial_a E^a = 0$  in free space, the last term goes away, and we are left with the familiar expression

$$H = \frac{1}{2} \int (\mathbf{B}^2 + \mathbf{E}^2) d^3\mathbf{x}, \quad (\text{A.52})$$

which is quite simply the energy stored in an electromagnetic field.

## B Simple Spin Networks and their Values

With the definitions and identities in Section 3, we can create a veritable panoply of spin networks. More importantly, we can assign numerical values to any closed spin network (since if a spin network is closed, we are effectively summing over all the indices of its component matrices.) Some important strand identities and closed spin networks, along with their values, are given in [27]; we cite these results here:

- The  $n$ -loop, denoted  $\Delta_n$ :

$$\bigcirc_n = (-1)^n (n+1) \quad (\text{B.1})$$

- The “theta”, denoted  $\theta(a, b, c)$ :

$$\bigcirc_{\theta}^a = (-1)^{(a+b+c)/2} \frac{\left(\frac{a+b+c}{2} + 1\right)! \left(\frac{a+b-c}{2}\right)! \left(\frac{b+c-a}{2}\right)! \left(\frac{c+a-b}{2}\right)!}{a!b!c!} \quad (\text{B.2})$$

Often, we will encounter a theta-diagram with two identical strands, and the third strand equal to 2. In this case, the value of the theta diagram becomes

$$\theta(m, m, 2) = (-1)^{m+1} \frac{(m+2)(m+1)}{2m} \quad (\text{B.3})$$

- The “Tet”, denoted  $\text{Tet} \begin{bmatrix} a & b & e \\ c & d & f \end{bmatrix}$ , whose value is given by

$$\begin{aligned} \text{Tet} \begin{bmatrix} a & b & e \\ c & d & f \end{bmatrix} &= \text{Diagram} \\ &= N \sum_{m \leq s \leq M} \frac{(-1)^s (s+1)!}{\prod_i (s - a_i)! \prod_j (b_j - s)!} \end{aligned} \quad (\text{B.4})$$

where

$$N = \frac{\prod_{i,j} (b_j - a_i)!}{a!b!c!d!e!f!}$$

$$a_1 = \frac{1}{2}(a + d + e) \quad b_1 = \frac{1}{2}(b + d + e + f)$$

$$a_2 = \frac{1}{2}(b + c + e) \quad b_2 = \frac{1}{2}(a + c + e + f)$$

$$a_3 = \frac{1}{2}(a + b + f) \quad b_3 = \frac{1}{2}(a + b + c + d)$$

$$a_4 = \frac{1}{2}(c + d + f)$$

$$m = \max\{a_i\} \quad M = \min\{b_j\}$$

- The “bubble” diagram, which is proportional to a single strand:

$$\begin{array}{c} | \\ a \\ \circlearrowleft \\ b \quad c \\ \circlearrowright \\ a' \\ | \end{array} = \delta_{aa'} \frac{\theta(a, b, c)}{\Delta_a} \begin{array}{c} | \\ a \\ | \end{array} \quad (\text{B.5})$$

- The lambda-move:

$$\begin{array}{c} | \\ c \\ \curvearrowright \\ a \quad b \\ \curvearrowleft \end{array} = \lambda_c^{ab} \begin{array}{c} | \\ c \\ \diagdown \\ a \quad b \end{array} \quad (\text{B.6})$$

where

$$\lambda_c^{ab} = (-1)^{(a(a+1)+b(b+1)-c(c+1))/2} \quad (\text{B.7})$$

- The *recoupling theorem*, which is perhaps the most important of these results:

$$\begin{array}{c} b \quad c \\ \diagdown \quad \diagup \\ i \\ \diagup \quad \diagdown \\ a \quad d \end{array} = \sum_i \left\{ \begin{array}{ccc} a & b & i \\ c & d & i' \end{array} \right\} \begin{array}{c} b \quad c \\ \diagdown \quad \diagup \\ i \\ \diagup \quad \diagdown \\ a \quad d \end{array} \quad (\text{B.8})$$

where the symbol on the right-hand side is the *Kauffman-Lins 6-j symbol*. Its value is given by

$$\left\{ \begin{array}{ccc} a & b & e \\ c & d & f \end{array} \right\} = \frac{\text{Tet} \begin{bmatrix} a & b & e \\ c & d & f \end{bmatrix} \Delta_e}{\theta(a, d, e)\theta(b, c, f)} \quad (\text{B.9})$$

The Kauffman-Lins 6-*j* symbols are related to the more commonly known Wigner 6-*j* symbols; for the details of this relation, see Appendix C.

- Given a 2-edge grasping one edge of a trivalent vertex, it is possible to “slide” it onto the other two edges, using the relation:

$$\begin{array}{c} p \quad q \\ \diagdown \quad \diagup \\ r \\ \diagup \quad \diagdown \\ \text{---} 2 \quad \text{---} \end{array} = p \begin{array}{c} p \quad q \\ \diagdown \quad \diagup \\ r \\ \diagup \quad \diagdown \\ \text{---} 2 \end{array} + q \begin{array}{c} p \quad q \\ \diagdown \quad \diagup \\ r \\ \diagup \quad \diagdown \\ \text{---} 2 \end{array} \quad (\text{B.10})$$

- A network with three edges branching from the vertices of a triangle can be written as a multiple of a simple trivalent vertex:

$$\begin{array}{c} a \quad k \quad b \\ \diagdown \quad \diagup \\ j \quad i \\ \diagup \quad \diagdown \\ c \end{array} = \frac{\text{Tet} \begin{bmatrix} a & b & c \\ i & j & k \end{bmatrix}}{\theta(a, b, c)} \begin{array}{c} a \quad b \\ \diagdown \quad \diagup \\ c \end{array} \quad (\text{B.11})$$

## C Relations Between Wigner 6- $j$ Symbols and Kauffman-Lins 6- $j$ Symbols

The Wigner 6- $j$  symbols, used in transformations between different couplings of three angular momenta, are very closely related to the Kauffman-Lins 6- $j$  symbols used in the recoupling theorem. Since the former of these symbols have been studied more thoroughly than the latter, it would be to our advantage to find a way to translate between them. However, there seems to be some confusion in the literature as to the proper translation. It can be shown, using the explicit formulas for the Wigner 6- $j$  symbol in Varshalovich [23] and the Kauffman-Lins 6- $j$  symbol in Kauffman and Lins [27], that

$$\left\{ \begin{array}{ccc} A/2 & B/2 & F/2 \\ C/2 & D/2 & E/2 \end{array} \right\}_W = \left\{ \begin{array}{ccc} A & B & E \\ C & D & F \end{array} \right\}_{KL} \cdot \frac{\sqrt{\theta(B, C, E)\theta(A, D, E)}}{\Delta_E \sqrt{\theta(A, B, F)\theta(C, D, F)}} \cdot (-1)^{(E+F)/2} \quad (C.1)$$

where the subscript  $KL$  indicates the Kauffman-Lins symbol and the  $W$  subscript indicates the Wigner symbol. Note the reversal of the arguments in the last column.

We will also have occasion to use the following identity, relating the Tet and the Wigner 6- $j$  symbol:

$$\left\{ \begin{array}{ccc} A/2 & B/2 & F/2 \\ C/2 & D/2 & E/2 \end{array} \right\}_W = \frac{\text{Tet} \left[ \begin{array}{ccc} A & B & E \\ C & D & F \end{array} \right]}{\sqrt{\theta(A, D, E)\theta(B, C, E)\theta(A, B, F)\theta(C, D, F)}} \quad (C.2)$$

In general, we will omit the  $KL$  subscript to indicate a Kauffman-Lins symbol; however, a Wigner 6- $j$  symbol will, in this work, always have the  $W$  subscript present.



## D Diffeomorphism Invariance & the Angle Spectrum

In our discussion of the definition and properties of spin networks, we scrupulously avoided any mention of what the exact nature of these networks might be. Specifically, we did not mention whether these networks are merely bookkeeping tools, embedded in an underlying spatial manifold and drawing on the properties of that manifold to give values to the operators; or whether this network has a deeper, more intrinsic structure. While our previous discussion proceeded without making this distinction, it is a natural question one might have about the theory; one might also wonder whether the properties of the angle operator presented here might shed some light on this subject.

One of the fundamental properties of general relativity is *diffeomorphism invariance*; in other words, the equations of general relativity are invariant under a certain class of smooth transformations known as diffeomorphisms. To get a better idea of what we mean by “smooth”, suppose we have an infinitely stretchable, unpuncturable balloon. If we were to squash it or stretch it, we would have a smooth transformation of the sheet. If, however, we were to pinch a point on the balloon and pull it up, it would *not* be a smooth transformation at this point of the sheet. (It would, however, be a smooth transformation at every other point of the balloon.)

An important property of these diffeomorphisms is that they are locally linear; in other words, if we look at a neighbourhood around any point of the aforementioned balloon, we can approximate the transformation as a linear transformation. Moreover, this approximation can be made to arbitrary accuracy by selecting a sufficiently small neighbourhood.

Suppose, then, that our balloon has a network drawn on it. If we examine a vertex of this network as we smoothly squash and stretch the balloon, we will see that the angles between the edges meeting at this vertex will change. It is evident, then, that diffeomorphisms can change the angle between two strands if they are embedded in an underlying manifold. However, our angle operator does not depend on any properties of the geometry of the strands, merely on their labels. This would seem to suggest, then, that the angle operator is diffeomorphism invariant.

There is another, more important conclusion to be drawn from the nature of the angle operator. The angle spectrum for any given vertex only includes a finite number of angles; even if we consider the set of all vertices with a given valence (a countable set), we would still only have a countable number of possible angles in this larger set. This is at odds with the classical continuum model of spacetime, which predicts that within the set of all  $n$ -vertices (where we consider a set of  $n$  rays originating at a point in space to be an  $n$ -vertex), there are an uncountable number of angles.

We could try to explain this uncountability away through diffeomorphism invariance; it is certainly conceivable that through adequate stretching & distorting of the surrounding space, we could turn any vertex into any other vertex;

at the very least, we might be able to define a countable set of equivalence classes of vertices, where two vertices are defined as equivalent if some diffeomorphism changes one vertex into the other.

Unfortunately, this is not the case. Grot and Rovelli [24] have shown that while any intersection of  $n$  lines in three-dimensional space can be deformed into any other intersection through arbitrary transformations of the underlying space, *linear* transformations cannot do so for an arbitrary intersection with  $n \geq 5$ . Instead, for  $n \geq 5$ , they show that if we define as equivalent two intersections which can be obtained from each other by a linear transformation, then there exist an uncountable number of equivalence classes of intersections. These equivalence classes can therefore be parameterized by at least one *continuous* parameter; Grot and Rovelli show that the dimension of this moduli space (i.e. the number of continuous parameters required) for vertices of valence  $n$  is given by

$$d(n) \geq (2n - 5)m - \frac{5}{2}m^2 - \frac{1}{2}m^3, \quad (\text{D.1})$$

where

$$m(n) = \left\lfloor \frac{\sqrt{48n - 23} - 7}{6} \right\rfloor. \quad (\text{D.2})$$

This formula yields  $d(n) \geq 0$  for  $n = 2, 3, 4$ , but  $d(5) \geq 2$ ,  $d(6) \geq 4$ , and increases without bound as  $n \rightarrow \infty$ . Grot and Rovelli also explicitly show (as an example) that  $d(5)$  is exactly equal to 2, and that the equivalence classes can be parameterized by the numbers

$$\lambda_1 = \frac{\angle_4^1 \angle_5^2}{\angle_4^2 \angle_5^1} \quad \text{and} \quad \lambda_2 = \frac{\angle_4^1 \angle_5^3}{\angle_4^3 \angle_5^1} \quad (\text{D.3})$$

where we have labelled the edges  $\{1, 2, 3, 4, 5\}$ , and  $\angle_j^i$  is the angle between edges  $i$  and  $j$ .

This result implies that even when we take diffeomorphism invariance into account, there is still an uncountable spectrum of possible “angles” for vertices with valence greater than or equal to 5. Of course, these parameters are only functions of what one might normally consider to be the angles of the vertex, as in (D.3); nevertheless, classical vertices under diffeomorphism still possess more degrees of freedom in possible angle values than the quantized angle operator would seem to allow.

What can we conclude from these facts? For vertices with  $n \geq 5$ , it should not surprise us that we have been reduced from an uncountably infinite number of possible measurements to a countably infinite number. After all, such a reduction occurs in many simple quantum mechanical systems, most notably in the measurements of angular momentum — in the classical picture, the angular momentum of a particle can take on any real value, while in the quantum picture, it must be an integer multiple of  $\hbar$ . The existence of these classical parameters may also imply, however, that the angle operator is “not all there

is”; if these parameters do persist in the quantum theory, then some (if not all) angle eigenvalues are highly degenerate.

The  $n = 3$  case, however, is much more surprising. In this case, the angle operator can still produce a countably infinite number of measurements (from the set of all trivalent vertices); these measurements are, as we showed above, diffeomorphism-invariant. However, under classical diffeomorphisms, a set of three vectors which span an  $m$ -dimensional space can be mapped to any other three vectors which also span an  $m$ -dimensional subspace. If  $m = 3$ , we have what Grot and Rovelli call the “non-degenerate” case; in this case, any two vertices are diffeomorphism equivalent. Grot and Rovelli also cite the result of Arnold [28] that this holds for the  $m = 2$  case as well. Finally, the  $m = 1$  case is trivial: the only possible classical angle measurements are  $0^\circ$  and  $180^\circ$ . Hence, there is only a *finite amount* of diffeomorphism-invariant information that can be extracted from a classical trivalent vertex! This is a drastic difference from the normal state of affairs in quantum mechanics; while quantizing a given theory normally *restricts* the amount of knowledge one can have about a system, the angle operator actually seems to be *increasing* it. This suggests that there is something fundamentally different going on at these low-valence vertices; the theory predicts that our naive continuum model of space breaks down at these tiny length scales.

## Acknowledgements

I would like to thank my advisor, Seth Major, for his invaluable help in the preparation of this thesis; without him, this work would certainly not have been possible. I would also like to thank my professors and fellow students at Swarthmore College, for four years of superb academic stimulation. Finally, I would like to thank my parents, for all of their support and encouragement over the past 21 years.

## References

- [1] Griffiths, David J. *Introduction to Electrodynamics*, 3<sup>rd</sup> edition. Prentice-Hall, Upper Saddle River, NJ, 1999.
- [2] Belot, Gordon. “Understanding Electromagnetism.” *Brit. J. Phil. Sci.*, **49**, 531-555 (1998).
- [3] Barrett, J. W. “Holonomy and Path Structures in General Relativity and Yang-Mills Theory.” *Int. J. Theo. Phys.*, **30**, 1171-1215 (1991).
- [4] Giles, R. “Reconstruction of Gauge Potentials from Wilson Loops.” *Phys. Rev. D* **24**, 2160 (1981).
- [5] Ashtekar, A. “New variables for classical and quantum gravity.” *Phys. Rev. Lett.* **57**, 2244 (1986).
- [6] Ashtekar, A. “New Hamiltonian formulation of general relativity.” *Phys. Rev. D* **36**, 1587-1602 (1987).
- [7] Sen, A. “Gravity as a Spin System.” *Phys. Lett.* **119B**, 69 (1982).
- [8] Immirzi, G. “Quantum Gravity and Regge Calculus”. *Nuc. Phys. Proc. Suppl.* **57**, 65-72 (1997). ArXiv ref. [gr-qc/9701052](#).
- [9] Rovelli, C. and L. Smolin. “Spin networks and quantum gravity.” *Phys. Rev. D* **52**, 5743-5759 (1995). ArXiv ref. [gr-qc/9505006](#).
- [10] Major, Seth A. “A Spin Network Primer.” *Am. J. Phys.* **67**, 972-980 (1999). ArXiv ref. [gr-qc/9905020](#).
- [11] Penrose, Roger. “Angular Momentum: An approach to combinatorial spacetime”, in *Quantum Theory and Beyond*, T. Bastin, ed. Cambridge University Press, Cambridge (1971).
- [12] De Pietri, Roberto and Carlo Rovelli. “Geometry Eigenvalues and the Scalar Product from Recoupling Theory in Loop Quantum Gravity.” *Phys. Rev. D* **54**, 2664-2690 (1996). ArXiv ref. [gr-qc/9602023](#).

- [13] Frittelli, S., L. Lehner, C. Rovelli. “The complete spectrum of the area from recoupling theory in loop quantum gravity” *Class. Quant. Grav.* **13**, 2921-2932 (1996). ArXiv ref. [gr-qc/9608043](#).
- [14] Rovelli, C. and L. Smolin, “Discreteness of area and volume in quantum gravity.” *Nuc. Phys.* **B 422**, 593 (1995); Erratum *Nuc. Phys.* **B 456**, 753 (1995). ArXiv ref. [gr-qc/9411005](#).
- [15] Major, Seth A. “Operators for Quantized Directions.” *Class. Quant. Grav.* **16**, 3859-3877 (1999). ArXiv ref. [gr-qc/9905019](#).
- [16] Loll, R. “Volume Operator in Discretized Quantum Gravity.” *Phys. Rev. Lett.* **75**, 3048-3051 (1995).
- [17] De Pietri, Roberto. “Spin Networks and Recoupling in Loop Quantum Gravity.” *Nucl. Phys. Proc. Suppl.* **57**, 251-254 (1997). ArXiv ref. [gr-qc/9701041](#).
- [18] Moussouris, John P. “Quantum Models of Spacetime Based on Recoupling Theory.” Ph.D. thesis, Oxford University, 1983 (unpublished.)
- [19] Edwards, Harold M. *Fermat’s Last Theorem: A Genetic Introduction to Algebraic Number Theory*. Springer-Verlag, New York, 1977.
- [20] Chrystal, G. *Algebra: An Elementary Textbook*. Dover Publications, New York, 1961.
- [21] Hilton, Peter and Jean Pedersen. “Catalan Numbers, their Generalization, and their Uses.” *Math. Int.* **13**, 64-79 (1991).
- [22] Bell, W.W. *Matrices for Scientists and Engineers*. Van Nostrand Reinhold Co., New York, 1975.
- [23] Varshalovich, D.A., A.N. Moskalev, V.K. Khersonskii. *Quantum Theory of Angular Momentum*. World Scientific, Teaneck, NJ, 1988.
- [24] Grot, Nobert and Carlo Rovelli. “Moduli-space structure of knots with intersections.” *J. Math. Phys.* **37**, 3014 (1996). ArXiv ref. [gr-qc/9604010](#).
- [25] Dirac, Paul A. M. *Lectures on Quantum Mechanics*. Belfer Graduate School of Science, Yeshiva University, New York, 1964.
- [26] Goldstein, Herbert: *Classical Mechanics*, 2<sup>nd</sup> edition. Addison-Wesley, Reading, MA, 1980.
- [27] Kaufmann, L. H. and S. L. Lins. *Temperley-Lieb Recoupling Theory and Invariants of 3-Manifolds*. Princeton University Press, Princeton, NJ, 1994.
- [28] Arnold, V.I. *Catastrophe Theory*. Springer-Verlag, Berlin, 1984.